

# Astrometric Detection of Terrestrial Planets in the Habitable Zones of Nearby Stars with SIM PlanetQuest

Joseph Catanzarite, Michael Shao, Angelle Tanner, Stephen Unwin, and Jeffrey Yu

*Jet Propulsion Laboratory, California Institute of Technology, 4800 Oak Grove Drive,  
Pasadena, CA 91109-8099*

[jcat@s383.jpl.nasa.gov](mailto:jcat@s383.jpl.nasa.gov)

## ABSTRACT

SIM (Space Interferometry Mission) PlanetQuest is a space-borne Michelson interferometer for precision stellar astrometry, with a nine meter baseline, currently slated for launch in 2015. One of the principal science goals is the astrometric detection and orbit characterization of terrestrial planets in the habitable zones of nearby stars. Differential astrometry of the target star against a set of reference stars lying within a degree will allow measurement of the target star's reflex motion with astrometric accuracy of  $\sim 1 \mu\text{as}$  in a single measurement.

The purpose of the present paper is to quantitatively assess SIM's capability for detection (as opposed to characterization by orbit determination) of terrestrial planets in the habitable zones of nearby solar-type stars. Note that the orbital periods of these planets are generally shorter than the five-year SIM mission. We formulate a "joint periodogram" as a tool for planet detection from astrometric data. For adequately sampled orbits, i.e., five or more observations per period, over a sampling timespan longer than the orbit period, we find that the joint periodogram is more sensitive than the  $\chi^2$  test for the null hypothesis. In our analysis of the problem, we use Monte Carlo simulations of orbit detection, together with realistic observing scenarios, actual target and reference star lists, realistic estimates of SIM instrument performance and plausible distributions of planetary system parameters.

Performance is quantified by three metrics: minimum detectable planet mass, number and mass distribution of detected planets, and completeness of detections in each mass range.

We compare SIM's performance on target lists optimized for the SIM and Terrestrial Planet Finder Coronograph (TPF-C) missions. Finally, we discuss the issue of confidence in detections and non-detections, and show how information from SIM's planet survey can enable TPF to increase its yield of terrestrial planets.

*Subject headings:* astrometry – instrumentation: interferometers – methods: data analysis – methods: statistical – planetary systems

## 1. Introduction

SIM will be the first instrument to use astrometry to detect and characterize terrestrial planets. The ability to make these detections depends on the performance of the instrument, the details of the observing scenarios, and the analysis of the astrometric data. This paper presents detailed simulations of the planet detection process. It includes a realistic model of the instrument performance, realistic observations of target and reference stars, and plausible distributions of the astrophysical parameters defining the ensembles of planetary systems. SIM is now at the end of NASA’s Phase B development. All significant technologies have been verified in laboratory testbeds, and the project is on track to build the flight instrument for launch as early as 2011. The instrument model in this paper is based on results from these testbeds.

Section 2 presents a brief description of SIM’s narrow angle observing scenario. Section 3 contains a discussion of the habitable zone and shows how the astrometric signature of a planet in the habitable zone of a main-sequence star scales with stellar luminosity and distance. In Section 4, we describe lists of SIM target stars and their characteristics, along with several possible survey modes which trade off number of stars versus number of observations per star. Section 5 provides a description of the joint periodogram technique for detection of periodicities in astrometric data. We describe the methodology of our study in Section 6. The main results are presented in Sections 6 and 7, in which we quantitatively characterize SIM’s sensitivity for detection of terrestrial planets, the expected mass distribution and total number of terrestrial planets SIM will discover, and the completeness of detected planets as a function of planet mass. In Section 8 we briefly consider how SIM’s discoveries can benefit the TPF mission.

## 2. Narrow-angle observing scenario

For narrow-angle astrometry, a target star should be surrounded by a group of reference stars located within a radius of about a degree. Differential delay measurements of the target and reference stars will be used to simultaneously estimate the position of the target star with respect to the reference frame and remove the linear field dependence in the delay measurements. (Yu 2002, Milman 2002, JPL internal memos). The least squares problem

involves three parameters, requiring a minimum of three reference stars. Ideally the target star is at the photo-center of the reference stars. For non-ideal reference star positions, there is a penalty on the position accuracy achievable on measurement of the target star with respect to the reference frame. It is best to have more than three reference stars per target star, since the more reference stars, the closer their photocenter is to the target star, and thus the lower the error penalty will be (assuming the distribution of reference star candidates is uniform on the sky near a target star). Selection of planet-search targets and their reference stars is discussed in Section 4. We find that most SIM planet-search targets have eight or more available bright K-giant reference star candidates within a kpc. According to our own simulations, we expect that four to six reference star candidates per target star will survive a ground-based radial velocity vetting program before SIM launches, and that of these, three or more will be astrometrically clean, i.e. will have astrometric reflex motion below SIM’s detection threshold.

For each visit to the target-reference group, the allocated integration time is divided into a sequence of “chopped” measurements, alternating between target and reference stars. In narrow-angle astrometry one is interested in the motion of the target star with respect to the reference stars, rather than in the absolute motion of the target star. Thus, a basic narrow-angle measurement is always a difference between delay measurements of two stars. Differences between successive target and reference star measurements are, to first order, free of common-mode errors and of linear temporal drift on the time scale of the chop. With optimally selected integration time, chopping serves to mitigate systematic time-dependent drifts (primarily due to changes in thermal environment). A *target-reference chop* is a 39-second delay measurement on the target star, followed by a 39-second delay measurement on the reference star. A *chop cycle* is a complete set of *target-reference chops*. For five reference stars the observing sequence for a *chop cycle* is  $T \rightarrow R_1 \rightarrow T \rightarrow R_2 \rightarrow T \rightarrow R_3 \rightarrow T \rightarrow R_4 \rightarrow T \rightarrow R_5 \rightarrow$ , where  $T$  and  $R_i$  refer to delay measurements of the target star and  $i^{th}$  reference star, respectively, and  $\rightarrow$  refers to a slew/settle/acquire sequence from either target to reference star or reference to target star. The last  $\rightarrow$  is a slew/settle/acquire back to the target star. Figure 1 illustrates SIM’s narrow-angle observing scenario. The slew/settle/acquire time between stars in the narrow-angle field is 15 seconds. A one-dimensional narrow-angle observation sequence, or *visit*, consists of two *chop cycles*, which comprises ten delay measurements on the target star, a total of ten delay measurements on the reference stars, and twenty slew/settle/acquisitions. At 39 seconds integration time per delay measurement, and 15 seconds per slew/settle/acquire, this totals 780 seconds integration on the target and reference stars, plus 300 seconds slew/settle/acquisition time, for a total mission time of 1080 seconds, or 0.3 hours per visit to a target.

The astrometric precision obtained in this one-dimensional narrow-angle observing se-

quence, for a bright ( $V < 7$ ) target star, or for the center of mass of the group of  $V < 10$  reference stars, is currently specified at  $1.0 \mu\text{as}$  (Yu 2005). This is subsequently referred to as SIM’s *single measurement accuracy*. This performance has been demonstrated in the Micro-Arcsecond Metrology (MAM) testbed at the Jet Propulsion Laboratory, and has been accepted by the SIM External Independent Review Team (EIRT). At  $1.0 \mu\text{as}$  single measurement accuracy, a differential measurement with 780 seconds total integration time divided among a  $7^{\text{th}}$  magnitude target star and set of  $10^{\text{th}}$  magnitude reference stars has astrometric accuracy of  $1.0 \times \sqrt{2} \mu\text{as}$ . This includes photon noise, instrument noise, and a multiplier that accounts for the geometric distribution of the reference stars (Yu 2005).

A two dimensional narrow-angle observation is a pair of *visits* (as described above) with the interferometer baseline oriented along quasi-orthogonal directions on the plane of the sky. For the first, and subsequent odd-numbered visits to the target-reference group, the interferometer baseline is oriented parallel to a reference direction on the plane tangent to the spacecraft boresight direction. For the second, and subsequent even-numbered visits to the target-reference group, the interferometer baseline is oriented along a direction in the tangent plane that is roughly orthogonal to the baseline orientation of the first observation. In this way, the two-dimensional motion of the target star on the plane of the sky is sampled. We assume even time sampling for the series of observations along each of the two baseline orientations, and that observation pairs are quasi-simultaneous, although the latter assumption is not strictly necessary.

In reality, scheduling constraints in the mission (including a solar exclusion zone) preclude even sampling. Sampling of SIM planet-search targets will be serendipitous, governed by their availability during repeated “orange-peel” scans of the sky, spiraling toward and away from the solar exclusion zone (Boden et al. 1997). Yearly gaps in the sampling ranging from several weeks to several months (for targets near the ecliptic) will occur during times when the target is in the solar exclusion zone.

(Ford 2004; Sozzetti et al. 2002) investigated planetary orbit detection with a number of sampling schemes. These include geometric, power law, and periodic with random gaussian perturbations, all with 24 two-dimensional observations. They found that all of these sampling schemes performed well, as long as the minimum gap between observations did not deviate too much from the average sampling interval. The most promising observing schedules were ‘periodic with perturbations’ of up to 40% of the average sampling interval (Ford 2004). Apart from annual sampling gaps due to the solar exclusion-zone, we expect actual sampling to be quasi-even, comparable to the ‘periodic with perturbation’ schemes investigated by (Ford 2004). We have not investigated the impact of these solar exclusion gaps on planet detectability. However, previous studies (Ford 2004; Sozzetti et al. 2002),

have shown that gaps much longer than the average sampling interval can attenuate detection at periods comparable to the survey length.

### 3. Terrestrial planets and the habitable zone

Terrestrial planets are defined as those composed primarily of silicate rock. In the solar system there are four (Mercury, Venus, Earth, and Mars), Earth being the most massive. Recent simulations of core accretion (Ida & Lin 2004) indicate that rocky planets form inwards of 3 AU from the parent star, and their masses can extend up to about 10 or 20  $M_{\oplus}$ . The upper mass limit results from the competition between core accretion and disk gas depletion. For the purpose of this study, we adopt a terrestrial planet mass range of one to ten  $M_{\oplus}$ .

The habitable zone is the region around a star in which liquid water, considered essential for life, can exist. Although life on Earth exists in environments much more extreme than this definition allows, feasible future missions such as the Terrestrial Planet Finder will be limited to studying the macroscopic physical and chemical properties of planets. From arguments based on Stefan’s Law, the Sun’s habitable zone is between 0.7 and 1.5 AU (Kasting et al. 1993). For the purpose of this study, we put the center of the Sun’s habitable zone at 1 AU. To remain inside the habitable zone, a planet with a semi-major axis of 1 AU should have eccentricity less than 0.35.

We define the occurrence rate  $\eta_{terrestrial}$  as the fraction of solar-type stars with terrestrial planets orbiting in their habitable zones. The mass distribution and occurrence rate of extrasolar terrestrial planets orbiting solar-type stars are at present unknown; only one candidate, at  $\sim 7.5 M_{\oplus}$  (Rivera et al. 2005) has been discovered to date. NASA’s Kepler mission (<http://www.kepler.arc.nasa.gov/>), scheduled to launch in 2009, will survey 100,000 solar-type stars (F, G and K dwarfs) over four years for transits of planets with masses between 0.5 and 10  $M_{\oplus}$ . By the time of the SIM launch, data from NASA’s Kepler mission may have yielded much information about the statistics of terrestrial planets orbiting inward of  $\sim 1$  AU. In any case, SIM will itself provide sufficient statistics to estimate the mass function and occurrence rate of terrestrial planets in habitable zones.

At the present time, the best approach is to extrapolate from the discoveries of radial velocity surveys. Masses of known extrasolar planets are roughly consistent with a power-law distribution  $dN/dM \propto M^{-1.1}$  (Tabachnik & Tremaine 2002; Marcy et al. 2005c), but they are generally tens to hundreds of times more massive than terrestrial planets. Nevertheless, the consistency of this power law with masses of solar system planets is evidence (albeit weak)

that it may also apply to terrestrial planets (Tremaine & Zakamska 2003). Integrating the power-laws for mass and period distributions (Tabachnik & Tremaine 2002) between 1 and  $10 M_{\oplus}$  and periods corresponding to orbit radii between 0.7 AU and 1.5 AU, we obtain an estimate of  $\eta_{terrestrial} = 0.013$ , or 1.3% for the occurrence rate of terrestrial planets in the habitable zones of solar-type stars. In the remainder of this work, we adopt the Tabachnik/Tremaine power law for terrestrial planet masses, assuming that each star has one terrestrial planet at mid-habitable zone, with mass drawn from the  $1/M^{1.1}$  distribution. Results can then be scaled to any value of  $\eta_{terrestrial}$ . In this work, we do not address the case of multiple-planet systems.

The habitable zone of a star scales with luminosity as

$$R_H = L_{\star}^{0.5}, \quad (1)$$

where  $R_H$  is the radius at mid-habitable zone in AU and  $L_{\star}$  is stellar bolometric luminosity in units of the solar bolometric luminosity  $L_{\odot}$ . The astrometric signature of a planet in the habitable zone is

$$\alpha'' = \frac{M_p}{M_{\star}} \frac{R_H}{D}, \quad (2)$$

where  $\alpha''$  is the angular size of the semi-major axis of the stellar reflex motion (if the orbit were seen face-on) in arcseconds,  $M_p$  and  $M_{\star}$  are planetary and stellar masses in solar units, respectively, and  $D$  is distance to the star in pc. Using Equation 1 for  $R_H$  in Equation 2 gives

$$\alpha'' = \frac{M_p}{M_{\star}} \frac{L_{\star}^{0.5}}{D}, \quad (3)$$

Most planet search targets are main sequence stars. A convenient form of the mass-luminosity relation for main-sequence stars with  $M_{\star} > 0.2$  is (Cox 2000, p. 132)

$$L_{\star} = M_{\star}^{3.8}. \quad (4)$$

Thus for main-sequence stars with  $M_{\star} > 0.2$ , the radius of the habitable zone scales with stellar mass as

$$R_H = M_{\star}^{1.9}. \quad (5)$$

More massive stars have larger habitable zones. A consequence for TPF-C (but not for SIM) is that for a fixed planet size, a larger habitable zone lowers the contrast ratio between the planet's reflected starlight and the star itself. Above a luminosity of  $5.4 L_{\odot}$ , corresponding to a habitable zone of radius 2.3 AU, and a stellar mass of  $1.6 M_{\odot}$ , the contrast ratio of a  $10 M_{\oplus}$  terrestrial planet falls below TPF-C's contrast limit of  $10^{-10}$ . From Equations 3 and

4, the astrometric signature of a planet in the habitable zone of a main-sequence star with  $M_\star > 0.2$  scales with stellar mass, planet mass, and distance as

$$\alpha'' = \frac{M_p M_\star^{0.9}}{D} \quad (6)$$

Evidently at fixed stellar distance, planets of a given mass in the habitable zones of more massive stars have larger stellar reflex motion signatures. These are the best targets for the SIM mission; but some of them will be unsuitable for TPF-C because of low contrast ratio. Targets for the TPF-C mission will be preferentially selected for large habitable zone angular size, subject to the contrast ratio constraint. In the next section, we discuss hypothetical SIM target lists, and their characteristics. In our simulations, we replaced Equation 4 with a slightly more accurate mass-luminosity relation (Griffiths et al. 1988), given by

$$\log_{10} L_\star = 4.20 \sin(\log_{10} M_\star - 0.281) + 1.174, \quad (7)$$

for  $-1 < \log_{10} M_\star < 1.25$ .

#### 4. Target lists for SIM planet surveys

Approximately 17% of SIM’s five-year mission time is designated for planet-searching in narrow-angle mode. Within this allocation, we consider three hypothetical survey modes, each of which uses all of SIM’s planet-finding time to observe targets brighter than 7<sup>th</sup> magnitude:

**Medium-Deep survey** – 240 target stars with 52 two-dimensional observations per target.

**Deep Survey** – 120 target stars with 104 two-dimensional observations per target.

**Ultra-Deep Survey** – 60 target stars with 208 two-dimensional observations per target.

All observations in these surveys are made at SIM’s nominal single measurement accuracy of 1.0  $\mu\text{as}$ . For each survey mode (except Medium-Deep, for which there are not enough TPF-C targets) we draw the stars from one of two target lists. The first is optimized for SIM, while the second is optimized for TPF-C.

Since virtually all likely SIM targets are known stars, it’s unnecessary to use synthetic stellar populations. Our hypothetical SIM-optimized target list is derived from an initial list of 2350 stars taken from the Hipparcos catalog with distances less than 30 pc (Turnbull & Tarter 2003). We removed all stars with  $V > 7$ , the limiting magnitude for the integration time assumed in the narrow-angle observing scenario. We removed those stars

with stellar companions within one arc-second of the primary star, to avoid contamination of the primary star’s fringe. We removed all stars with stellar companions orbiting with semi-major axis within a factor of ten of the radius of the mid-habitable zone of the primary star. This is a conservative limit at which a companion will not have a significant gravitational effect on a planet within the habitable zone (Holman & Weigert 1999). We screened out possible giant stars by the following process. Stars catalogued as luminosity class III in SIMBAD were removed if they had luminosity consistent with a giant star, but kept if their luminosity was consistent with a dwarf. Stars catalogued as dwarfs were removed if they had luminosity exceeding that expected of a dwarf star. After these cuts, the 575 remaining stars were sorted in descending order of the stellar astrometric signature that would be induced by an Earth-mass planet at mid-habitable zone. Finally, to optimize for detection of terrestrial planets in the habitable zone, stars whose orbit periods at mid-habitable zone were longer than five years or shorter than 0.2 years (the period corresponding to Nyquist sampling of 50 observations over five years) were removed from the list. After this cut, the list contained 545 stars. The top 60, 120 and 240 stars on this list are the targets for the Ultra-Deep, Deep and Medium-Deep surveys, respectively.

For the hypothetical TPF-C targets, we used a list of 384 stars (Burrows 2005). This list was derived from the Hipparcos database (Turnbull & Tarter 2003). It comprises all single F, G, or K main sequence stars brighter than 7<sup>th</sup> magnitude, closer than 30 pc, and with  $B - V$  colors in the range 0.3 to 1.4. Two further constraints are imposed: the mid-habitable zone must be outside of TPF-C’s Inner Working Angle of 62 mas, and the luminosity of the star must be less than  $5.4 L_{\odot}$ , so that the contrast ratio exceeds  $10^{-10}$  for a terrestrial planet of  $10 M_{\oplus}$ . Of the 384 stars in the list, about 120 survived application of these constraints, so for the TPF-optimized list, there is no Medium-Deep survey. These stars were then ranked in descending order of star-planet angular separation for a planet at mid-Habitable zone. For the Ultra-Deep and Deep TPF-C surveys we chose the best 60 and 120 stars, respectively, from this final list. We note that these are not necessarily the best targets for the TPF-Interferometer mission (TPF-I). TPF-I has a smaller inner working angle, and could potentially detect planets in the much smaller habitable zones of M-stars.

Histograms of V magnitude and orbital period at mid-habitable zone for the best 120 TPF-C targets and for the best 240 SIM targets are shown in Figures 2 and 3. Note the wider range of mid-habitable zone periods in the SIM target list, which has been selected for large habitable zones.

Reference stars are K-giants selected from the Tycho 2 and 2MASS catalogs (Tanner et al. 2006). The following criteria were used:

1. They should be K Giant stars which are luminous and therefore distant, in order to

minimize gravitational perturbations due to planetary companions. Reduced Proper Motion, defined as  $RPM = K_S + 5\log(\mu)$  serves as a proxy for distance. We require  $RPM < 1$ .

2. They should have an infrared color range  $0.5 < J - K_S < 1.0$
3. They should have an optical color range  $1.0 < B - V < 1.5$ .
4. They should lie within a 1.25 degree radius of the target star
5. They should be bright:  $V < 10$  to minimize observing time
6. They should have favorable geometry: we choose four reference stars in each quadrant around target if possible

Our planet-search target and reference stars have not been screened for photometric variability, which may be an indicator of starspot activity. (Sozzetti 2005; Hatzes 2002) have modeled photocenter shifts due to starspots; their results show that for typical planet search targets, large spots causing a flux change of 1% can induce photocenter shifts of the same order as astrometric reflex motion due to terrestrial planets in the habitable zone. (Sozzetti 2005) notes that since the effect correlates strongly with photometric variability, photometric screening and/or monitoring of planet-search targets should be considered. An average sunspot group contains about ten sunspots, each with an area of about 0.04% of the Sun’s disk.(Cox 2000). The presence of simultaneous multiple starspots tends to randomize the photocenter shift. For a solar-type target star at 10 pc, we find, in agreement with (Sozzetti 2005), that 0.1% flux variations due to a single starspot introduces a photocenter shift with amplitude of  $\sim 0.3 \mu\text{as}$ . While larger starspots may be possible, we believe that since the photometric shift due to starspots is color-dependent whereas reflex motion is not, spectral information provided by SIM observations will serve to break the degeneracy.

We consider also the problem of photocenter shifts in reference stars. (Henry et al. 2000) performed a survey of 187 F, G, and K giants for photometric variability . They found that photometric variability exhibits a strong color dependence; for giants meeting our selection criterion of  $1.0 < B - V < 1.5$ , most exhibit maximum flux variations of well under 1%. They concluded that for giants cooler than K2III, the observed photometric variation is most likely due to radial stellar pulsations (which cause no photocenter shift) rather than starspots. If, however, we assume that the observed photometric variation is due entirely to starspots, a simple starspot model shows that photocenter shift of K giants at 1 kpc is expected to be well under 0.4 uas. Our conclusion is that starspots are not a major concern for reference stars.

## 5. The joint periodogram: a tool for astrometric detection of planets

The standard method of detecting periodicity in one-dimensional time series data is the Lomb-Scargle periodogram (Scargle 1982). The Lomb-Scargle periodogram and its variants are widely used in detection of planets in radial velocity data (Cumming 2004; Cumming et al. 1999; Nelson & Angel 1998; Walker et al. 1995). Discussion of the application of the periodogram to detection of planets in astrometric data is found in (Black & Scargle 1982), and (Sozzetti et al. 2003) have investigated using the periodogram to detect multiple planets in astrometric data.

The Lomb-Scargle periodogram is readily extended to detection of periodicity in two-dimensional astrometric data time-series. We define the joint periodogram as the sum of the Lomb-Scargle periodogram power of the astrometric signal in the two independent channels associated with the orthogonal baseline orientations of the SIM interferometer. There is no requirement on the maximum time interval between a measurement in one channel and the corresponding measurement in the other channel. Detection of a planet is registered when its joint power exceeds a detection threshold set according to the desired false-alarm level.

Measurements in each channel are assumed uniformly sampled in time. Comparison of many sampling schemes shows that apart from the aliasing problem, even sampling is best for detection of orbits with periods shorter than the length of the survey (Ford 2004). In our use of the periodogram, we have sidestepped aliasing effects by counting any signal that exceeds the detection threshold as a detection, regardless of whether the detected and actual periods match. Thus our analysis should yield detection efficiencies comparable to those found using other sampling schemes that are optimized to reduce aliasing (Ford 2004; Sozzetti et al. 2002). Our use of even sampling in the simulations is mainly for convenience in the analysis.

The joint periodogram uses all the information in both channels of the astrometric data for planet detection and period estimation. It is ideally suited for detection of well-sampled circular orbits with period shorter than the time baseline of the observations. For elliptical orbits, detection efficiency is reduced for two reasons: power leaks into the overtones of the orbit frequency, and for certain orbit geometries, the full astrometric signature of the stellar reflex motion is not observed. However, we find that these effects are not significant for the relatively small eccentricities ( $e < 0.35$ ) we consider. Our simulations show that the joint periodogram detects Keplerian orbits with higher efficiency than using separate periodograms on the two channels.

A necessary preliminary step in any detection scheme is to establish the false-alarm probability (FAP) corresponding to a range of detection thresholds. The false-alarm probability

corresponding to a given detection threshold (periodogram power) is the likelihood that pure Gaussian noise would produce a periodogram peak whose power exceeds the detection threshold. Lowering the detection threshold raises the false-alarm probability. In our simulations, we determined detection thresholds corresponding to various false-alarm probabilities using 100,000 Monte Carlo realizations of the no-planet case, where the simulated observations consist purely of Gaussian measurement noise. For the purpose of discovering planets in radial velocity data, a 1% false-alarm probability is commonly required (Marcy et al. 2005b). Detection of a signal exceeding the threshold corresponding to a 1% false-alarm probability is said to be at a 99% significance level.

For sufficiently small values, the false-alarm probability is proportional to the number of independent frequencies scanned in the periodogram (Horne & Baliunas 1986; Press, et al. 1992). For  $N$  evenly-spaced observations in the time series, the range of detectable frequencies is spanned by the  $N/2$  independent frequencies  $\{ \frac{1}{T}, \frac{2}{T}, \dots, \frac{N}{2T} \}$ , where  $T$  is the time between the first and last measurement (nominally five years for the SIM mission), and  $\frac{N}{2T}$  is the Nyquist frequency. But to adequately sample a peak, the periodogram must be scanned at a finer frequency interval. Our Monte Carlo experiments show, in agreement with Horne & Baliunas (1986) and Press, et al. (1992) that the effective number of independent frequencies is  $\sim N$ , rather than  $N/2$ , because of this oversampling. Evidently, limiting the range of frequencies over which the periodogram is scanned increases the detection efficiency at a given confidence level. For the results presented in this paper, we chose to sample the periodogram down to periods as low as 0.2 years (semi-major axis of 0.34 AU for a planet orbiting a solar-mass star) corresponding to the Nyquist frequency for 50 samples evenly spaced in time over a five-year mission. Figure 4 is a plot of the FAP versus detection threshold, from a Monte Carlo ensemble of 100,000 realizations of a series of 50 two-dimensional observations, evenly spaced over five years of Gaussian noise, at 1  $\mu\text{as}$  single-measurement error. The 1% FAP threshold corresponds to astrometric signal of 1.36  $\mu\text{as}$ .

## 6. Detection of terrestrial planets in the habitable zones of nearby stars with SIM

In this section we determine SIM’s sensitivity for detection of terrestrial planets in the habitable zone, for hypothetical SIM and TPF-C target lists. For each target list and survey strategy, we answer the question: what is the distribution of minimum detectable mass for terrestrial planets in the habitable zone?

We first generate Keplerian reflex motion orbits for a Monte Carlo sample of solar-mass stars at 10 pc, each with a single terrestrial planet (i.e. a planet with mass in the range 1

to  $10 M_{\oplus}$ ). We determine the detection efficiency as a function of planet mass. Then we extend this result, deriving a universal detection efficiency curve for a star of arbitrary mass, luminosity and distance, and observed with arbitrary number of two-dimensional measurements and differential measurement error. From the universal detection efficiency curve, we develop a semi-analytical formula for minimum detectable mass of terrestrial planets in the habitable zone. For each survey strategy (and its hypothetical target list), we determine SIM’s sensitivity for detection of terrestrial planets in the habitable zone, for each target star.

These results provide a description of the sensitivity of the SIM instrument for detecting terrestrial mass planets orbiting in the habitable zones of nearby stars; they are independent of assumptions concerning the occurrence rate and mass distribution of terrestrial planets. Detailed results and discussion are presented in §6.2.

### 6.1. Monte Carlo sample

The starting point is a Monte Carlo simulation of astrometric detection of planets in the habitable zone of a solar-type star at a distance of 10 pc, in order to determine detection efficiency as a function of planet mass. Detection efficiency at a given planet mass is defined as the likelihood that a planet of that mass will be detected in the presence of measurement noise. For each planet mass in the range 0 to  $10 M_{\oplus}$ , at intervals of  $0.5 M_{\oplus}$ , we generate 10,000 realizations of Keplerian orbits with a one-year period, around a solar-mass star at 10 pc. Eccentricity is uniformly distributed between zero and a maximum of 0.35, consistent with orbits lying entirely within the habitable zone. We randomly draw other orbit parameters (inclination, longitude of ascending node, longitude and time of periastron) from their allowed domains. For each realization of an orbit, we generate a time series of 50 two-dimensional astrometric observations of the star’s position, evenly spaced in time over a five-year time period. Each observation is perturbed with  $1 \mu\text{as}$  Gaussian measurement error. In these initial simulations, we did not account for the effects of parallax and proper motion.

We employ the joint periodogram to detect periodic stellar reflex motion indicating the presence of a planet. Detection efficiency at a given mass and FAP is defined as the fraction of the ensemble of Keplerian orbit realizations for which the joint periodogram power exceeds the detection threshold associated with this FAP.

At moderate signal, a detection threshold corresponding to the peak of the periodogram power distribution corresponds roughly to 50% detection efficiency – noise is equally likely to add to the signal, raising it above the threshold, or subtract from the signal, pushing

it below the threshold (since the distribution of periodogram power is nearly symmetric). Increasing or decreasing the detection threshold by the same increment results in equal and opposite changes in the number of detected planets (see Figure 5).

Figure 6 shows SIM’s detection efficiency (for detection thresholds corresponding to false-alarm probabilities of 1% and 5%) as a function of planet mass for the fiducial case of terrestrial planets in one-year orbits around a solar-type star at a distance of 10 pc. Note that as required, in the limit as the signal approaches zero, the detection efficiency approaches the false-alarm probability.

## 6.2. SIM planet detection sensitivity

If we assume that detection efficiency is independent of orbit period, then it should depend only on the signal-to-noise ratio (SNR). This is expected to hold when there are sufficiently many observations, the orbit period is shorter than the observation time baseline, and the data do not include the effects of parallax and proper motion. We define the SNR of the astrometric data as

$$SNR = \frac{\alpha \sqrt{N_{obs}}}{\sqrt{2}\sigma}, \quad (8)$$

where  $\alpha$  is the angular size of the semimajor axis of the orbit in  $\mu as$ , if it were viewed in a face-on orientation,  $N_{obs}$  is the number of two-dimensional observations of the star, and  $\sigma$  is the single-measurement accuracy in  $\mu as$ . A factor of  $\sqrt{2}$  occurs in the denominator because narrow-angle measurements are differential (§2). The SIM technology testbeds have demonstrated that SNR improves with  $N_{obs}$  according to Equation (8) up to  $N_{obs} \geq 100$ . Substituting for  $\alpha$  using  $\alpha''$  from Equation 3 (remembering to convert from arcseconds to micro-arcseconds), converting planet mass from solar-mass to earth-mass units, and using the mass-luminosity relation of Equation 4, we have:

$$SNR = 3.004 \cdot M_p \frac{L_\star^{0.24}}{D} \frac{\sqrt{N_{obs}}}{\sqrt{2}\sigma}, \quad (9)$$

where  $M_p$  is planet mass in units of  $M_\oplus$ , and  $D$  is the distance to the target star in pc.

Universal detection efficiency curves comparing detection via the joint periodogram and the  $\chi^2$  test are shown in Figure 7. For the  $\chi^2$  test, detection is registered when the  $\chi^2$  test warrants a rejection of the null (no-planet) hypothesis. The curves are derived from a Monte Carlo ensemble of solar-mass stars at 10 pc, each with a planet in a one-year orbit, with eccentricities in the range  $0 < e < 0.35$ , observed 50 times along each of two orthogonal

baseline directions with  $1 \mu\text{as}$  single measurement error. We have confirmed via additional Monte Carlo simulations for cases of 24, 100, and 200 two-dimensional observations over five years, that detection efficiency versus SNR curves are indeed identical.

We find that the joint periodogram is more sensitive than the  $\chi^2$  test of the null hypothesis for detection of planets in Keplerian orbits (see Figure 7). Our simulations indicate that this result is generally valid for well-sampled data, when the orbit period is shorter than the survey duration. A reason may be that since Gaussian noise has a flat frequency spectrum, the  $\chi^2$  test is sensitive to noise at all frequencies. By contrast, periodogram power includes only noise at the natural frequencies near the detected peak.

SIM planet detection sensitivity for a target can conveniently be expressed in terms of minimum detectable planet mass. For the purpose of discovering planets in radial velocity data, a 1% false-alarm probability (FAP) is commonly required (Marcy et al. 2005c). For each target star, we define a minimum detectable mass to be the minimum mass of a planet orbiting in the habitable zone, detectable at 1% false-alarm probability with 50% detection efficiency.

As an example of how detection efficiency and FAP are related, consider Figure 7. At SNR of  $\sim 5.4$ , the detection efficiency is 50% at 1% FAP, for planets with eccentricity uniformly distributed in the range  $0 < e < 0.35$ . According to Equation 9, SNR of  $\sim 5.4$  corresponds to a minimum detectable mass of  $3.6M_{\oplus}$ , for 50 two-dimensional observations of a solar-mass star at 10 pc, with single-measurement precision of  $1 \mu\text{as}$ . Figure 6 shows this graphically: 50% detection efficiency occurs for a planet mass of  $3.6 M_{\oplus}$ . More generally, Equation 9 evaluated at SNR = 5.4 relates the minimum detectable mass to the number of observations, single-measurement precision, distance and luminosity of the star. Comparison with the case of 50 observations at  $1 \mu\text{as}$  single-measurement precision for a solar-type star at 10 pc yields a useful semi-analytical scaling law for the minimum detectable mass  $M_{p,min}$  of a terrestrial planet in the habitable zone of a main-sequence star:

$$M_{p,min} = 3.6M_{\oplus} \frac{\sigma}{1 \mu\text{as}} \sqrt{\frac{50}{N_{obs}}} \frac{D}{10 \text{ pc}} \frac{1}{L_{\star}^{0.24}}, \quad (10)$$

where  $N_{obs}$  is the number of 2-dimensional observations,  $\sigma$  is the single-measurement accuracy in  $\mu\text{as}$ ,  $D$  is the distance to the star in pc, and  $L_{\star}$  is the bolometric stellar luminosity in solar units.

### 6.3. Correction for effects of parallax and proper motion

In the foregoing development, we implicitly assumed that detection efficiency is independent of orbit period. But when the effects of parallax and proper motion are accounted for, detection probability is attenuated for orbit periods approaching one year (due to confusion of the orbit trajectory with parallax), and also for orbit periods approaching the five-year observation window (due to confusion of the orbit trajectory with proper motion). For discussions and studies of these effects, see (Black & Scargle 1982; Lattanzi et al. 2000; Sozzetti et al. 2002; Ford 2004). We need to revise our approach in order to account for sensitivity to orbit period. To characterize the effect, we generated sets of Monte Carlo ensembles for the same range of planet masses as reflected in Figure 6. Instead of putting every star at 10 pc and every planet at orbit period of 1 year as before, we generated ensembles of planets, with each ensemble having a fixed orbit period chosen from a range of values between 0.2 and 5 years; for each period we adjusted the distance to keep the astrometric signal the same as if the planet were in a 1 AU orbit around a solar mass star 10 pc away. We fitted the observations of each star to a model for parallax (at ecliptic latitude of  $30^\circ$ ) and proper motion before running the periodogram search. Examples of correction to detection efficiency as a function of period, for several values of SNR are shown in Figure 8. The marked reduction in detection efficiency for periods in the range 0.8 to 1.2 years is due to confusion of stellar reflex motion with parallax. Confusion of reflex motion with proper motion causes falloff in detection efficiency with increasing period. To fully account for sensitivity to period, we used the results of our Monte Carlo simulations to construct a lookup table for detection efficiency as a function of SNR and orbit period. For any target star, given the number of observations and measurement noise, and the orbit period at its mid-habitable zone, a detection efficiency curve (similar to Figure 6, but corrected for the effects of parallax and proper motion) is obtained by interpolation in this table.

Figure 9 shows a histogram of the corrections to minimum detectable mass for the Medium-deep survey; note that although for some stars the correction can be quite large, the corrections for most stars are  $< 0.25M_\oplus$ .

From the detection efficiency curve for any target star (now corrected for the effects of parallax and proper motion) we can determine the minimum detectable mass of a terrestrial planet in the habitable zone of that star. In all plots and tables to follow, minimum detectable mass has been corrected for the effects of parallax and proper motion.

#### 6.4. Results for minimum detectable planet mass

By the time SIM launches in 2015, the ubiquity of terrestrial planets orbiting solar-type stars may already be known from discoveries of the Kepler mission. For a fixed amount of SIM mission time, the optimum number of stars to survey for planets with SIM depends on the abundance of Earth-mass planets in the local Galactic environment. For example, if terrestrial planets turn out to be relatively rare, a reasonable strategy for SIM is to survey a larger number of stars with correspondingly fewer observations per star. To explore this trade, we consider the Medium-Deep, Deep, and Ultra-Deep survey modes, described in §4, which use the same amount of SIM mission time to observe different numbers of targets.

For the hypothetical SIM target list, Figures 10, 11A and 12A show histograms of the minimum detectable mass for the Medium-Deep, Deep and Ultra-Deep surveys of the best SIM targets. Figures 11B and 12B show distributions of minimum detectable masses for the Deep and Ultra-Deep surveys for the best TPF-C targets. There is no Medium-Deep survey for the TPF-C target list, since there are only  $\sim 120$  stars meeting the requirements that the habitable zone lie outside the inner working angle of 62 mas and close enough to the star so that the contrast exceeds  $10^{-10}$ . The main results of this study are presented in Figures 21 and 22. These figures show the mass limits of SIM planet detection, comparing cumulative distributions of minimum detectable mass for surveys of the best TPF-C and SIM targets, respectively. These results are summarized in Table 1. Figures 13A and 14AB show minimum detectable mass versus stellar distance. Figures 13B and 15AB show minimum detectable mass versus star-planet separation at mid-habitable zone. We find that SIM can probe the best 60, 120 and 240 planet search targets down to planet masses of 2, 4, and  $7 M_{\oplus}$ , respectively. It is important to note that these results depend only on assumptions about the SIM instrument. They do not depend on the astrophysics of planet mass distribution and occurrence frequency.

#### 6.5. Comparison with earlier studies

Several previous studies (Sozzetti et al. 2002; Sozzetti et al. 2003; Ford & Tremaine 2003) have addressed SIM’s detection and orbital characterization capabilities. These studies employed the  $\chi^2$  test rather than the periodogram for planet detection. A detection is registered when the  $\chi^2$  test warrants a rejection of the null (no-planet) hypothesis. The studies of Sozzetti et al. adopt a significance level of 95% when determining whether a planet has been detected. They define a scaled signal  $S$ , as the ratio of the astrometric amplitude,  $\alpha$ , and the single measurement astrometric accuracy,  $\sigma_d$ . They determine that  $S$  must be greater than 2.2 to detect a planet with 95% probability, and assume that SIM will make only 24

2-D observations per star surveyed. Other points of difference between their work and this work are: they assume that planetary orbits span the full range of eccentricities; we focus only on planets in the habitable zone; they assume a single measurement accuracy of  $2 \mu\text{as}$  (and higher, for faint stars).

Ford & Tremaine (2003) generally accept the (Sozzetti et al. 2002) conclusions regarding SIM’s detection efficiency. They further investigate the issue via similar Monte Carlo simulations for planets around stars of spectral types F, G, K and M, within 100 pc and up to a V magnitude of 10.5. They consider a range of single measurement accuracies of 1, 1.4, and  $2 \mu\text{as}$  associated with samples of 120, 240, and 480 stars. They also consider a two-tier observing strategy with the first tier of stars measured to  $1 \mu\text{as}$  accuracy and the second tier measured to  $4 \mu\text{as}$  accuracy; they consider both five and ten year missions. As in this work, they adopt the power-law planet mass distribution (Tabachnik & Tremaine 2002) consistent with currently known planets discovered by the radial velocity method.

We believe that the results of the present study represent a better estimate of SIM’s likely science return in this field, for two reasons. First, we have realistically modeled the likely SIM performance and observing scenario, taking total observation time into consideration. Second, the joint periodogram represents a more effective method of extracting planetary signals from astrometric data than the  $\chi^2$  test of the null hypothesis.

## 7. Discovery of terrestrial planets by SIM

In this section we address two further questions: What is the mass distribution and number of planets SIM will discover? What is SIM’s completeness for detection of terrestrial planets in the habitable zone, i.e., what fraction of the terrestrial planet discovery space does SIM probe?

To answer these questions, additional (astrophysical) assumptions are needed. We first extrapolate the mass distribution of currently known planets (Tabachnik & Tremaine 2002) to terrestrial planet masses. Next, for each target list and survey strategy, we use the universal detection efficiency curve to determine the detection efficiency versus planet mass for each target star. These two relations allow us to determine the expected mass distribution of terrestrial planets SIM will detect. This can be compared with the expected mass distribution of existing planets. In each mass bin, the completeness is defined to be the ratio of the number of detected planets to the number of expected planets. With an assumed value of  $\eta_{\text{terrestrial}}$  (defined as the fraction of F, G, and K stars having terrestrial planets in their habitable zones) we can also estimate the expected *number* of terrestrial planets SIM will

discover in each mass bin. Detailed results in the form of tables and plots are presented in the next two subsections.

### 7.1. What is the mass distribution and number of planets SIM will discover?

Our starting point is the universal detection efficiency versus SNR curve for each star in the hypothetical target lists, as discussed in the previous section. From Equation 3,  $\alpha$  depends on distance, stellar mass, planet mass, and luminosity (through size of the habitable zone). Given these parameters, together with values for  $N_{obs}$  and  $\sigma$ , we can derive a relation between detection efficiency and planet mass for each star in the target list. To proceed further, we evaluate the hypothetical case that each star has one terrestrial planet at its mid-habitable zone, with mass drawn at random from the distribution  $dN/dM \propto M^{-1.1}$  (Tabachnik & Tremaine 2002; Marcy et. al 2005a).

The expected probability distribution function for a detected planet at a given mass is the product of detection efficiency and  $dN/dM$ , at that mass. The probability distribution function has a peak, since it is the product of the monotonically decreasing planet mass distribution and the monotonically increasing, S-shaped detection efficiency versus mass curve.

Summing the expected probability distribution functions for all the stars in the target list gives the distribution of the number of terrestrial planets discovered per unit mass interval. Integrating over unit mass bins from 1 to  $10 M_{\oplus}$  gives a histogram of the number of planets discovered in each mass bin. Results for the three survey modes for the SIM target list are shown in Figures 16A, 17A, and 18A; corresponding results for surveys involving the TPF-C target list are shown in Figures 19A and 20A. The results are summarized in Table 2. These results are for the case of  $\eta_{terrestrial} = 1$ , and are easily scaled to any other value of  $\eta_{terrestrial}$ .

Integrating the distribution of number of terrestrial planets discovered per unit mass interval up to mass  $M$  gives the cumulative distribution for the total number of planets discovered up to mass  $M$ . Figures 23 and 24 show results for surveys of the best TPF-C and SIM targets, respectively. These plots reveal the relative merits of the three survey strategies. For both target lists, the Ultra-Deep survey nets more low-mass terrestrial planets, but fewer total discoveries. For the SIM target list, the Medium-Deep survey finds the most planets, but with the distribution skewed toward higher masses.

## 7.2. What fraction of the terrestrial planet discovery space does SIM probe?

For each mass bin, we determine completeness, which is the ratio of detected planets to the number of expected planets. We also determine cumulative completeness, the ratio of the number of detected planets below mass  $M$  to the number of expected planets below mass  $M$ . Completeness depends on our assumption that the probability distribution function (pdf) of terrestrial planet masses is  $\propto M^{-1.1}$ ; however no assumption about  $\eta_{terrestrial}$  is needed. Figures 16B, 17B, and 18B show completeness for Medium-Deep, Deep, and Ultra-Deep surveys of the best SIM targets. For these surveys, SIM detects nearly all planets above 9, 5, and  $3 M_{\oplus}$ , respectively. Figures 19B and 20B show completeness for Deep and Ultra-Deep surveys of the best TPF-C targets. For these surveys, SIM finds nearly all the terrestrial planets more massive than 7 and  $4 M_{\oplus}$ , respectively.

One important conclusion is that for all three survey modes, SIM will find essentially all planets above  $9 M_{\oplus}$  residing in the habitable zones of target stars. This may be a significant population of planets; simulations in Ida & Lin support a maximum terrestrial planet mass of up to  $20 M_{\oplus}$  for core accretion models. Recently discovered Neptune-mass planets (Butler et.al. 2004; McArthur et al. 2004) may be the first indication of that population, since they both reside inside the orbits of gas giants (Boss 2005).

Cumulative completeness for surveys of the best TPF-C and SIM targets is shown in Figures 25 and 26, respectively. We find that SIM will detect 32%, 56%, and 80% of terrestrial planets below  $10 M_{\oplus}$ ; and 6%, 22%, and 60% of terrestrial planets below  $3 M_{\oplus}$  for the Medium-Deep, Deep and Ultra-Deep surveys, respectively.

## 8. How SIM discoveries will benefit TPF

The Terrestrial Planet Finder (TPF) mission is being designed to have the capability to directly detect terrestrial planets in the habitable zones of nearby stars. In particular, the coronograph mission TPF-C shall be able to detect a potentially habitable planet around at least 100 nearby stars (TPF & SIM Synergy White Paper 2005). While TPF-C can do this in the absence of apriori information, achievement of its scientific priorities will undoubtedly be furthered by knowledge of planetary statistics from Kepler, and detections of terrestrial planets by SIM.

SIM's observations of TPF-C targets provide potentially valuable information for the TPF mission. SIM's minimum detectable mass for a target provides a lower limit for a detected planet's mass, while the orbit period provides the star-planet separation. SIM will also yield information about the *confidence in a detection* – the probability that a planet

is present in the case of a positive detection; and the *confidence in a non-detection* – the probability that a planet is absent, in the case of a non-detection. It is straightforward to apply Bayes' rule to determine these quantities. Results (averaged over the best 120 TPF-C targets observed in a Deep survey) are shown in Figure 27. See Appendix A for a discussion.

If SIM detects a planet at a given candidate TPF-C target star, the minimum planet mass detectable by SIM, the star-planet separation, together with the degree of confidence that a terrestrial planet is present allows the TPF mission to assign a quantitative priority for observing this potential target. On the other hand, if no planet is detected by SIM, then the degree of confidence that no terrestrial planet exists, together with SIM's and TPF's minimum detectable masses again can help prioritize this target for TPF. For example, at a given target, if the confidence that no terrestrial planet exists is high, and TPF's minimum detectable mass is higher than SIM's, the target would be given a very low priority.

For many stars with terrestrial planets, SIM will also characterize the orbits, providing estimates of inclination, eccentricity, and semimajor axis, allowing specification of optimal times and mirror orientations for TPF observations. Because SIM detects planets dynamically, it can unambiguously measure the planet's mass. SIM's potential for astrometric orbit characterization and planet mass determination has been addressed comprehensively in (Ford & Tremaine 2003; Sozzetti et al. 2003; Sozzetti et al. 2002).

## 9. Summary and Conclusions

We introduced the joint periodogram and showed that it is more sensitive than the  $\chi^2$  test for the null hypothesis for planet detection. We derived a semi-empirical relation for minimum detectable planet mass in terms of stellar distance and luminosity, number of measurements over five years, and instrument noise. We showed how this relation can be corrected for the effects of parallax and proper motion. Using actual SIM target lists we determined SIM's sensitivity for detection of terrestrial planets in the habitable zones of nearby stars. For the Medium-Deep, Deep, and Ultra-deep surveys of the best SIM target stars within 30 pc, we

1. Evaluated the median minimum detectable mass for a planet at mid-habitable zone. For surveys of the best 240, 120, and 60 SIM target stars, we determine median minimum detectable planet masses of  $5.3$ ,  $2.9$  and  $1.6 M_{\oplus}$ , respectively.
2. Determined the expected mass distribution and total number of terrestrial planets that SIM will discover. If each target star has a terrestrial planet orbiting within its habitable zone, we find that for surveys of the best 240, 120, and 60 SIM target stars,

SIM will discover 77, 68, and 48 terrestrial planets, with mean mass of 6.2, 5.2, and  $4.3 M_{\oplus}$  respectively; of these, 7, 13, and 18 planets, respectively, will have mass below  $3M_{\oplus}$ .

3. Determined the completeness of SIM’s terrestrial planet discoveries (i.e., the ratio of detected planets to expected planets) as a function of planet mass. For the three specified surveys of the best SIM targets, we find that SIM detects 32%, 56%, and 80% of terrestrial planets below  $10M_{\oplus}$ ; and 6%, 22%, and 60% of terrestrial planets below  $3M_{\oplus}$ .

Finally, we discussed the confidence in SIM detections and non-detections, and described how information from SIM’s planet survey can enable Terrestrial Planet Finder (TPF) to increase its yield of terrestrial planets.

We are grateful to Serge Dubovitsky, Debra Fischer, Chris Gelino, Andy Gould, Geoff Marcy, Chris McCarthy, Bijan Nemati, and Stuart Shaklan for helpful discussions and/or other contributions to this work. We wish to thank an anonymous referee for a most thorough critical review, with many recommendations that greatly improved the paper. This work was carried out at the Jet Propulsion Laboratory, California Institute of Technology, under contract with NASA.

### A. Confidence in a detection or non-detection

Given the occurrence rate  $\eta_{terrestrial}$  for terrestrial planets, the false-alarm probability  $F$  at the detection threshold, and the probability  $P_{det}$  that an existing terrestrial planet will be detected, we can use Bayes’ Rule to determine the confidence in a detection (i.e., the probability that a detection is not a false positive) at a given target star.

Formally, Bayes’ rule for the confidence in a detection is:

$$p(TP \text{ exists}|TP \text{ detected}) = \frac{p(TP \text{ detected}|TP \text{ exists}) \times p(TP \text{ exists})}{p(TP \text{ detected})}, \quad (\text{A1})$$

where TP stands for terrestrial planet and (in accordance with standard usage) the symbol  $|$  means *conditioned on*, or *given*. The denominator of the right-hand side of equation (A1) can be expanded as  $p(TP \text{ detected}) = p(TP \text{ detected}|TP \text{ exists}) \times p(TP \text{ exists}) + p(TP \text{ detected}|TP \text{ } \overline{\text{exists}}) \times p(TP \text{ } \overline{\text{exists}})$ . Recognizing that  $p(TP \text{ detected}|TP \text{ } \overline{\text{exists}}) \equiv F$ ,  $p(TP \text{ detected}|TP \text{ exists}) \equiv P_{det}$ ,  $p(TP \text{ exists}) \equiv \eta_{terrestrial}$  and  $p(TP \text{ } \overline{\text{exists}}) \equiv 1 - \eta_{terrestrial}$ , we rewrite the denominator of the right-hand side of Equation (A1) as  $p(TP \text{ detected}) =$

$P_{det} \times \eta_{terrestrial} + F \times (1 - \eta_{terrestrial})$ , and the numerator as  $P_{det} \times \eta_{terrestrial}$ . The confidence in a detection is therefore

$$p(TP \text{ exists} | TP \text{ detected}) = \frac{P_{det} \times \eta_{terrestrial}}{P_{det} \times \eta_{terrestrial} + F \times (1 - \eta_{terrestrial})} \quad (\text{A2})$$

Similarly, the confidence in a non-detection (i.e., the probability that a non-detection is not a missed detection) at a given target star can also be expressed in terms of Bayes' rule, as follows:

$$p(TP \overline{\text{exist}} | TP \overline{\text{detected}}) = \frac{p(TP \overline{\text{detected}} | TP \overline{\text{exist}}) \times p(TP \overline{\text{exist}})}{p(TP \overline{\text{detected}})} \quad (\text{A3})$$

The denominator of the right-hand side of (A3) can be expanded as  $p(TP \overline{\text{detected}}) = p(TP \overline{\text{detected}} | TP \overline{\text{exist}}) \times p(TP \overline{\text{exist}}) + p(TP \overline{\text{detected}} | TP \text{ exists}) \times p(TP \text{ exists})$ . Finally, since  $p(TP \overline{\text{detected}} | TP \overline{\text{exist}}) \equiv 1 - F$ , and  $p(TP \overline{\text{detected}} | TP \text{ exists}) \equiv 1 - P_{det}$ , the confidence in a non-detection becomes

$$p(TP \overline{\text{exist}} | TP \overline{\text{detected}}) = \frac{(1 - F) \times (1 - \eta_{terrestrial})}{(1 - F) \times (1 - \eta_{terrestrial}) + (1 - P_{det}) \times \eta_{terrestrial}} \quad (\text{A4})$$

In practice the confidences would be computed on a star-by-star basis. Figure 27 shows confidences in a detection and in a non-detection, respectively, averaged over all targets, for a Deep survey of the best 120 TPF-C targets. If  $\eta_{terrestrial}$  is 0.1, then for detection threshold corresponding to 1% false-alarm probability, average confidence in a detection is 82% and average confidence in a non-detection is 94%. The former result means that we are 82% certain, on average, that a detection is really a terrestrial planet in the habitable zone and not a false positive. The latter result means that on average, we are 94% certain that a non-detection rules out the existence of terrestrial planet in the habitable zone.

## REFERENCES

Black, D.C. and Scargle, J.D. 1982 *ApJ*, 263, 854

Boden, A., Unwin, S., & Shao, M. 1997, in *Proceedings of the ESA Symposium SP-402* (Venice: ESA)

Boss, Alan, private communication

Burrows, Chris, private communication

Butler, R. P., et al. 2004, *ApJ*, 617, 580

Cox, A.N., ed. 2000 *Allen's Astrophysical Quantities* 4th ed., (New York: Springer)

Cumming, A. 2004, *MNRAS*, 354, 1165

Cumming, A., Marcy, G.M., & Butler, R.P. 1999, *ApJ*, 526, 890

Ford, E. B. & Tremaine, S. 2003, *PASP*, 115, 1171

Ford, E. B. 2004, *AJ*, 129, 1706

Griffiths, S. C., Hicks, R. B. & Milone, E.F. 1988, *J. Roy. Astron. Soc. Can.*, Vol. 82, No. 1

Tanner, A., Gelino, C., Catanzarite, J., and Shao, M., in preparation

Hatzes, A.P. 2002 *Astron. Nachr.*, 323, 392

Henry, G. W., et al. 2000, *ApJS*, 130, 201

Holman, M. & Wiegert, P. 1999, *AJ*, 117, 621

Horne, J.H., & Baliunas, S. L. 1986, *ApJ*, 302, 757

Ida, S. & Lin, D. N. C. 2004, *ApJ*, 604, 338

Kasting, J.F., Whitmire, D.P. & Reynolds, R.T. 1993, *Icarus*, 101, 108

Lattanzi, M.G., Spagna, A., Sozzetti, A., and Casertano, S. 2000, *MNRAS*, 317, 211

<http://www.kepler.arc.nasa.gov/>

Marcy, G.W., Fischer, D.A., McCarthy, C. & Ford, E.B. 2005, in *ASP Conf. Ser. 338, Astrometry in the Age of the Next Generation of Large Telescopes*, ed. P. K. Seidelmann and A. K. B. Monet (San Francisco: ASP)

Marcy, G.W., et al. 2005, ApJ, 619, 570

Marcy, G.W., et al. 2005, Progress of Theoretical Physics Supplement 158, 24

McArthur, B. E., et al. 2004, ApJ, 614, L81

Nelson, A.F., Angel, J.R., 1998 ApJ, 500, 940

Press, W.H., et al. 1992, Numerical Recipes in C, 2nd. ed., (Cambridge: Cambridge University Press)

Rivera, E., et al. 2005, ApJ, 634, 625

Scargle, J.D. 1982, ApJ, 263, 835

Sozzetti, A., Casertano, S., Brown, R.A. & Lattanzi, M.G. 2002, PASP, 114, 1173

Sozzetti, A., Casertano, S., Brown, R.A. & Lattanzi, M.G. 2003, PASP, 115, 1072

Sozzetti, A. 2005, PASP, 117, 1021

Tabachnik, S. & Tremaine, S. 2002, Mon. Not. R. Astron. Soc., 335, 151

[http://planetquest.jpl.nasa.gov/documents/synergy\\_finalNew.pdf](http://planetquest.jpl.nasa.gov/documents/synergy_finalNew.pdf)

Tremaine, S. & Zakamska, N. 2003, in AIP Conf. Proceedings 713, The Search for Other Worlds: Fourteenth Astrophysics Conference, ed. S.S. Holt & D. Deming (College Park: AIP)

Turnbull, M. C., & Tarter, J. C. 2003, ApJS, 149, 423

Walker, G.A., Walker, A. R., Irwin, A.W., Larson, A.M., Yang, S.L., Richardson, D.C. 1995, Icarus, 116, 359

Yu, Jeffrey 2005, SIM PlanetQuest astrometric error budget.

Table 1. Number of Detected Planets versus Minimum Mass <sup>†</sup>

Min Mass	SIM Ultra-Deep	SIM Deep	SIM Medium-Deep	TPF Ultra-Deep	TPF Deep
$10 M_{\oplus}$	60	120	240	60	120
9	60	120	240	60	120
8	60	120	240	60	120
7	60	120	240	60	120
6	60	120	179	60	120
5	60	119	101	60	110
4	60	114	55	60	62
3	60	64	23	60	34
2	55	20	6	30	11
1.5	23	7	4	12	4
1	6	4	3	3	2

<sup>†</sup>For 50% detection efficiency and 1% false-alarm probability

Table 2. SIM terrestrial planet discoveries<sup>†</sup>

Survey	Median min. detectable mass	$< 10 M_{\oplus}$	$< 3 M_{\oplus}$	Mean mass
Best 60 for SIM	$1.6 M_{\oplus}$	48	18	$4.3 M_{\oplus}$
Best 60 for TPF	$2.0 M_{\oplus}$	42	13	$4.6 M_{\oplus}$
Best 120 for SIM	$2.9 M_{\oplus}$	68	13	$5.2 M_{\oplus}$
Best 120 for TPF	$4.0 M_{\oplus}$	54	8	$5.6 M_{\oplus}$
Best 240 for SIM	$5.3 M_{\oplus}$	77	7	$6.2 M_{\oplus}$

<sup>†</sup>Assuming each target has a terrestrial planet, with masses distributed as  $M^{-1.1}$  (Tabachnik & Tremaine 2002)

## Narrow-angle observing scenario

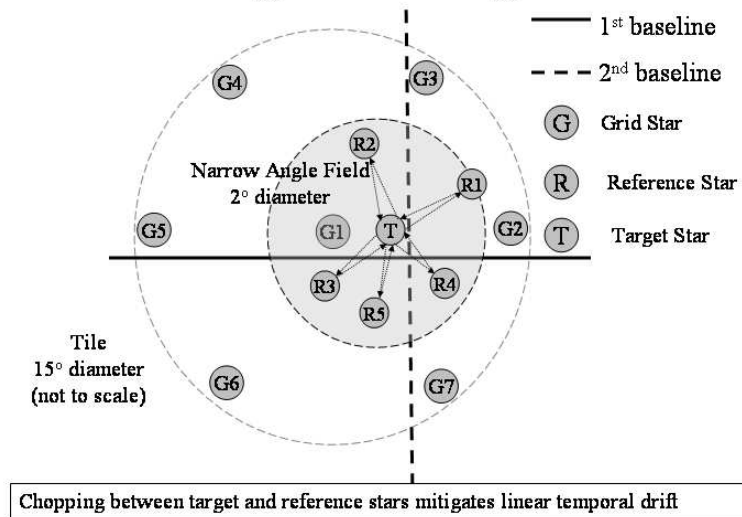


Fig. 1.— Narrow-angle observing scenario for planet surveys

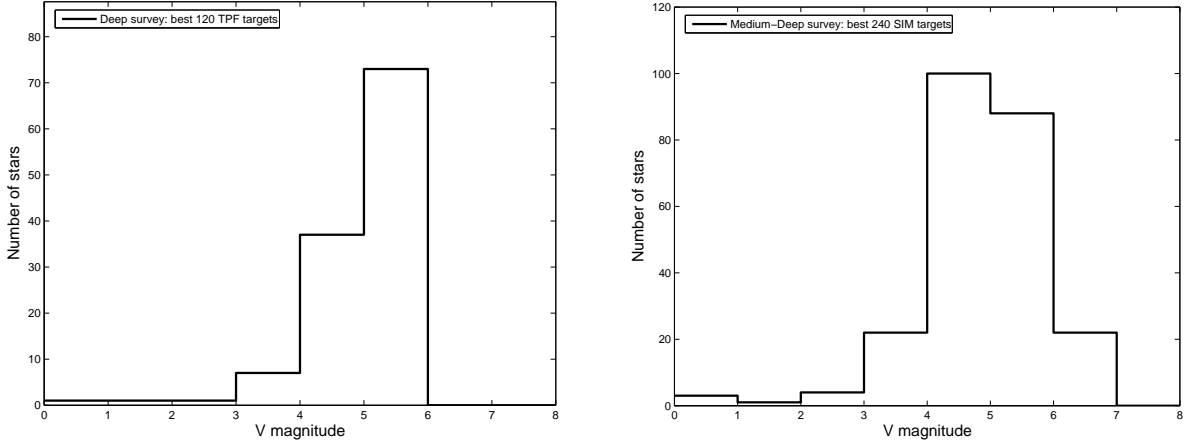


Fig. 2.— V magnitudes. Left: Best 120 TPF target stars. Right: Best 240 SIM target stars.

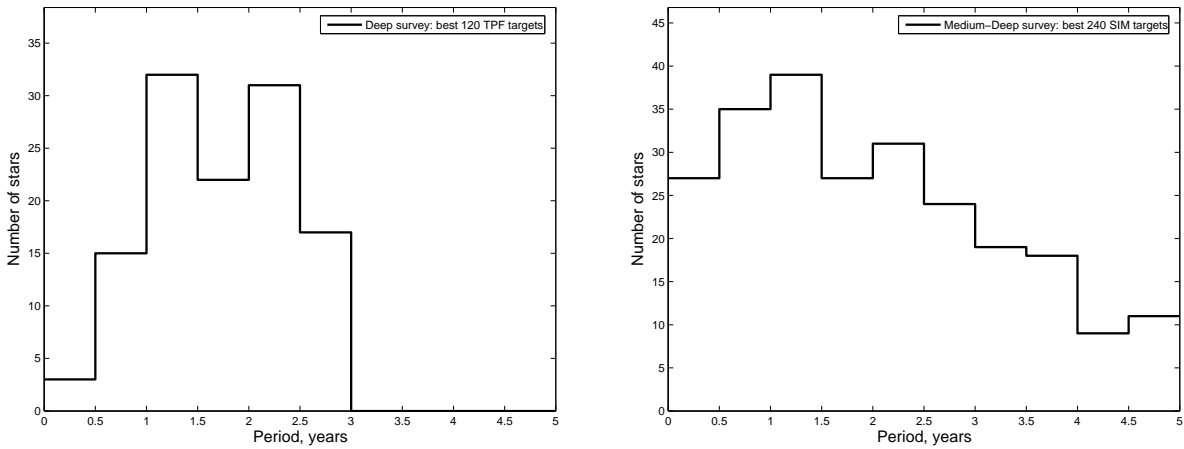


Fig. 3.— Orbital period at mid-habitable zone. Left: Best 120 TPF target stars. Right: Best 240 SIM target stars.

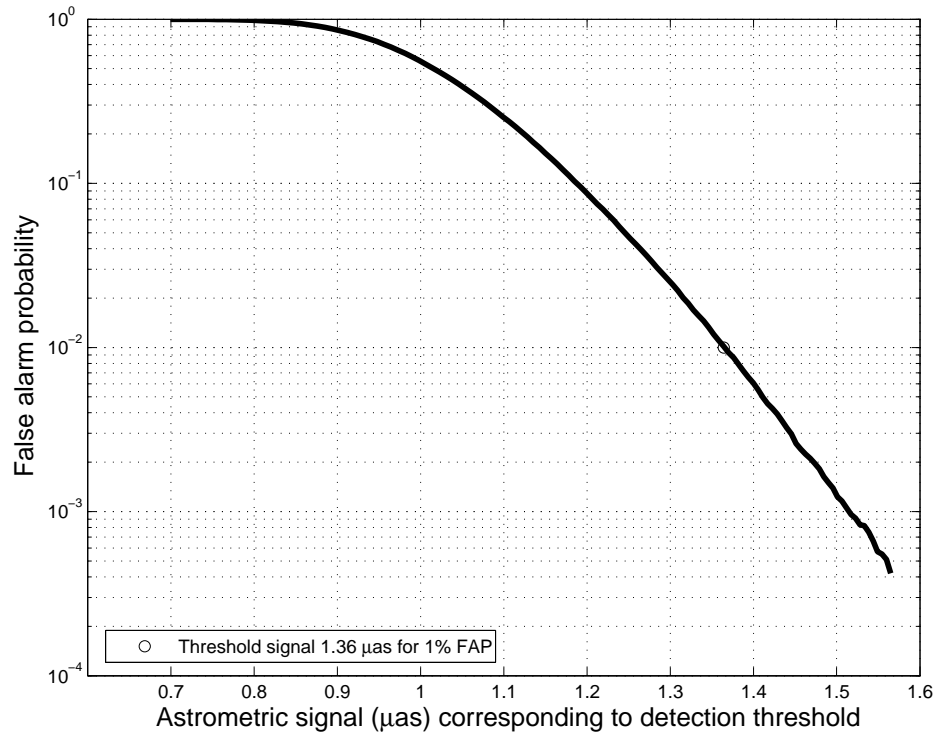


Fig. 4.— False-alarm probability versus signal detection threshold for the joint periodogram: 100,000 trials, 50 two-dimensional observations per star, evenly sampled over five years at single measurement precision of 1  $\mu\text{as}$ .

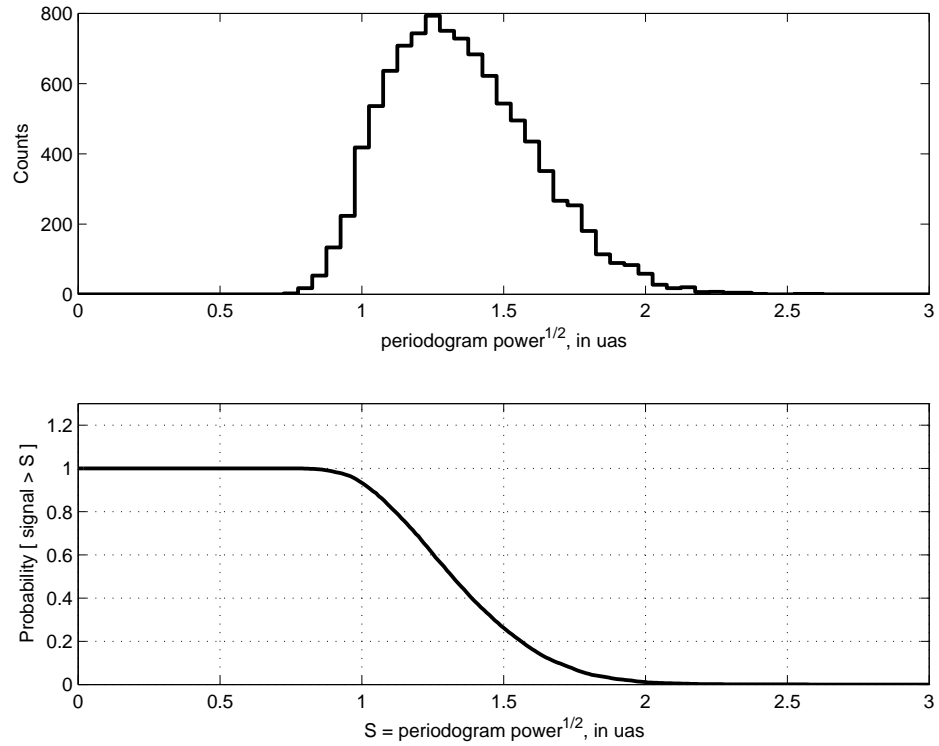


Fig. 5.— Upper panel: Periodogram power distribution for an ensemble of 10,000 realizations of a  $3.5 M_{\oplus}$  planet in a one-year orbit around a solar-mass star at a distance of 10 pc. Five-year mission, 50 evenly sampled two-dimensional observations at  $1 \mu\text{as}$  single measurement precision. Lower panel: Detection efficiency versus detection threshold (normalized integral of the power distribution)

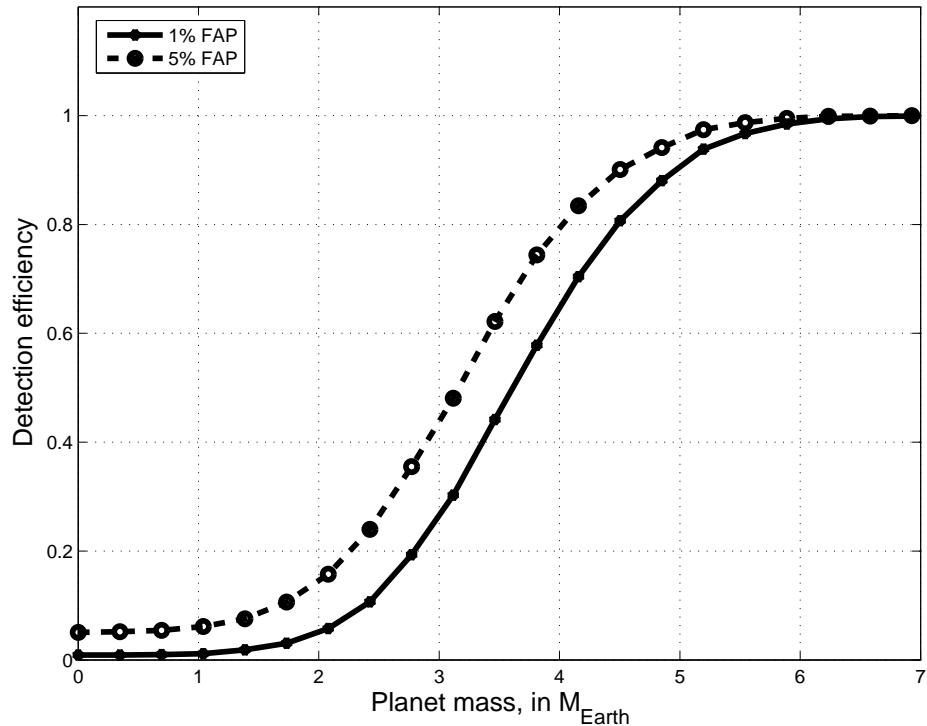


Fig. 6.— Detection efficiency versus planet mass for a terrestrial planet in a one-year orbit around a solar-mass star at a distance of 10 pc. Five-year mission, 50 two-dimensional observations per star at single measurement precision of  $1 \mu\text{as}$ ; orbital eccentricities in the range  $0 < e < 0.35$ . Each data point represents an ensemble of 10,000 Monte Carlo orbits. Not corrected for the effects of proper motion and parallax.

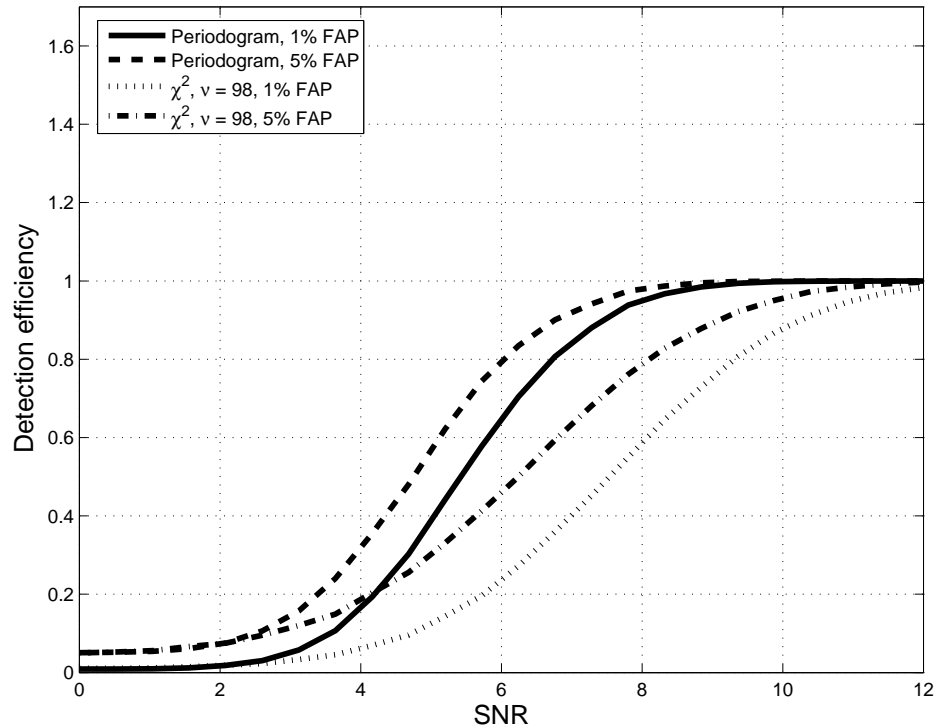


Fig. 7.— Universal SIM detection efficiency curves for periodogram versus  $\chi^2$  detection. Based on Monte Carlo simulations with 50 2D observations of orbits with eccentricities in the range  $0 < e < 0.35$ . Not corrected for the effects of proper motion and parallax.

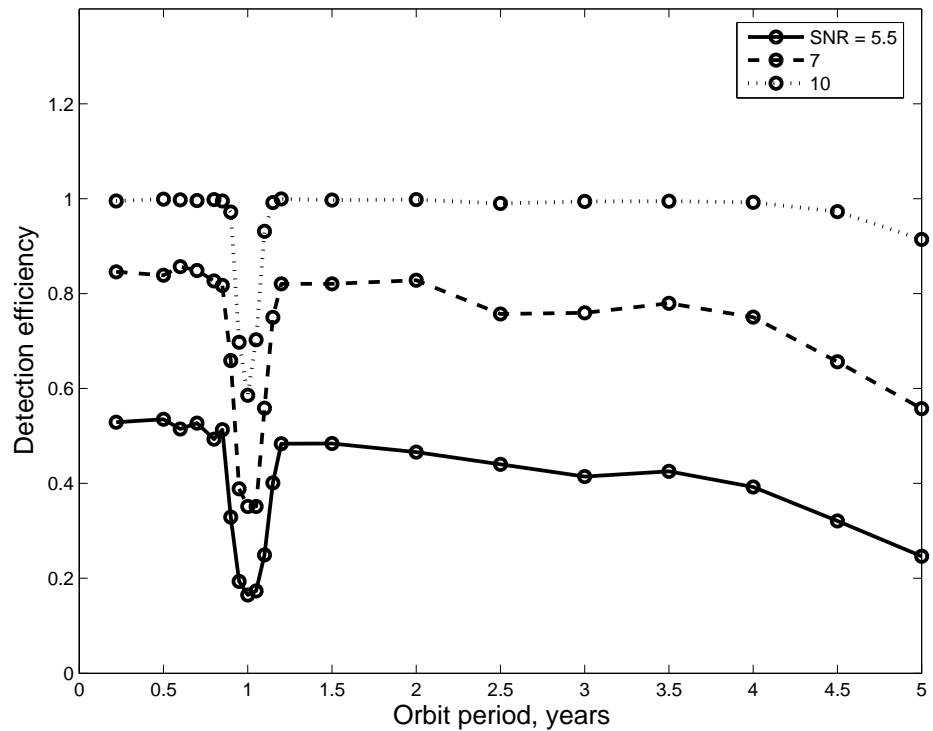


Fig. 8.— Sensitivity of periodogram detection to period, for several values of signal-to-noise ratio (SNR). Each data point represents an ensemble of 1000 Monte Carlo orbits. The loss in sensitivity near orbit periods of one year is due to confusion of stellar reflex motion with parallax; the steep decline at longer orbit periods is due to confusion of stellar reflex motion with proper motion. Detection threshold corresponds to 1% false-alarm probability.

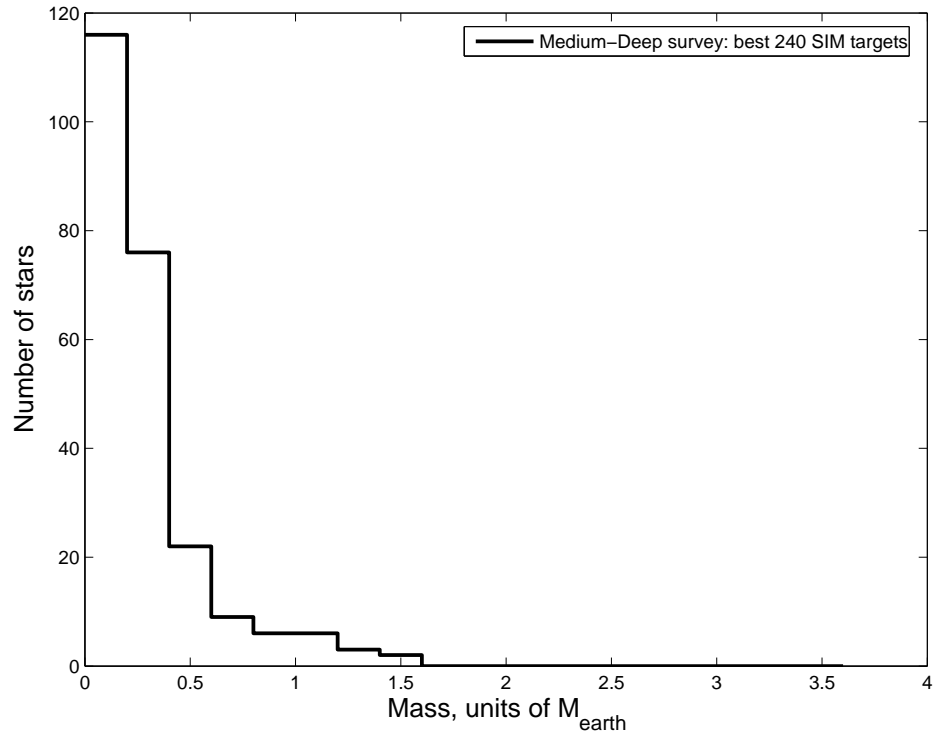


Fig. 9.— Correction to minimum detectable mass due to parallax and proper motion. Medium-Deep planet survey – best 240 stars for SIM, 52 two-dimensional measurements per star. Single measurement precision is 1.0  $\mu\text{as}$ ; minimum detectable mass is for 50% detection efficiency at detection threshold corresponding to 1% false-alarm probability.

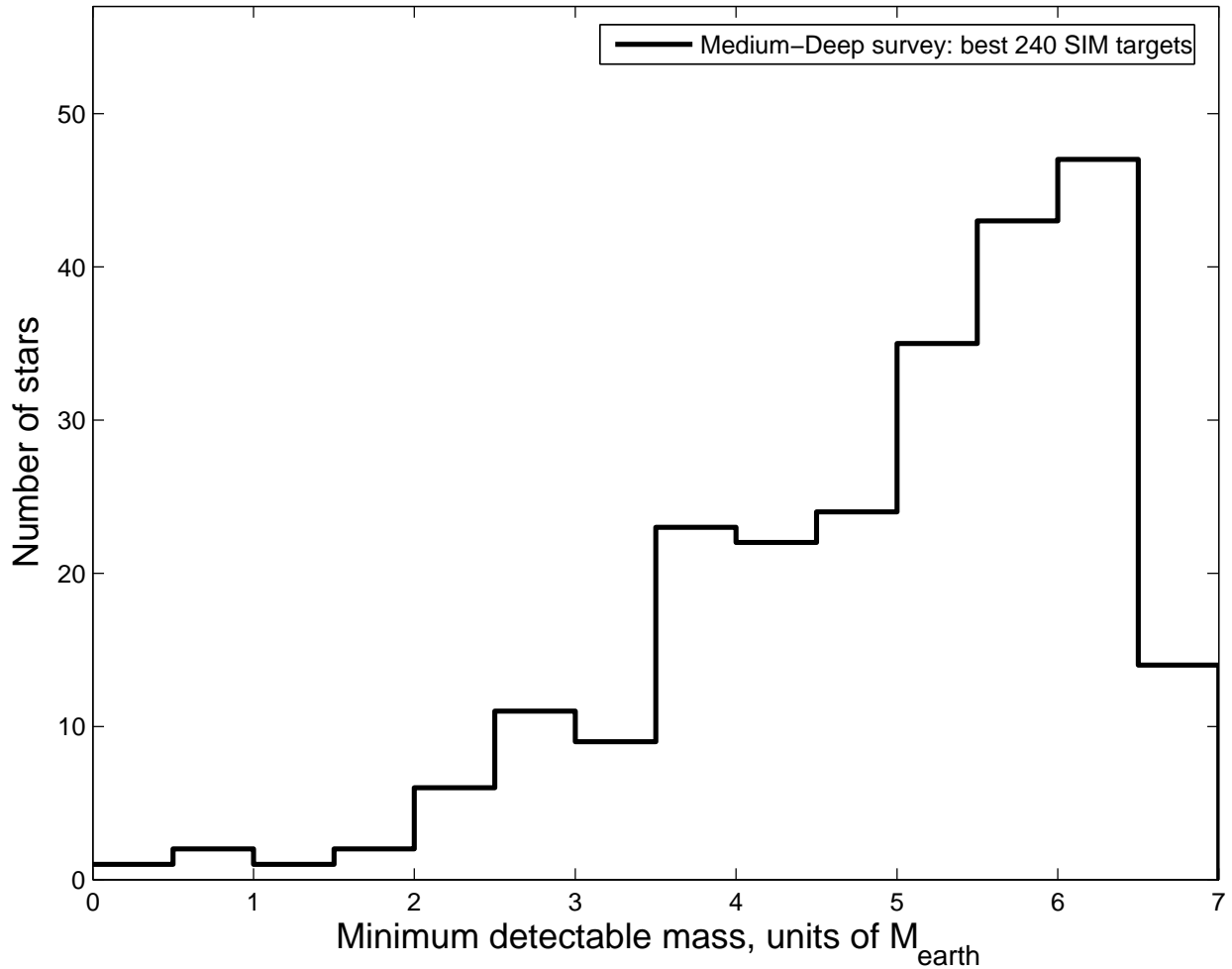


Fig. 10.— Distribution of minimum detectable masses. Medium-Deep planet survey – best 240 stars for SIM, 52 two-dimensional measurements per star. Single measurement precision is  $1.0 \mu\text{as}$ ; minimum detectable mass is for 50% detection efficiency at detection threshold corresponding to 1% false-alarm probability.

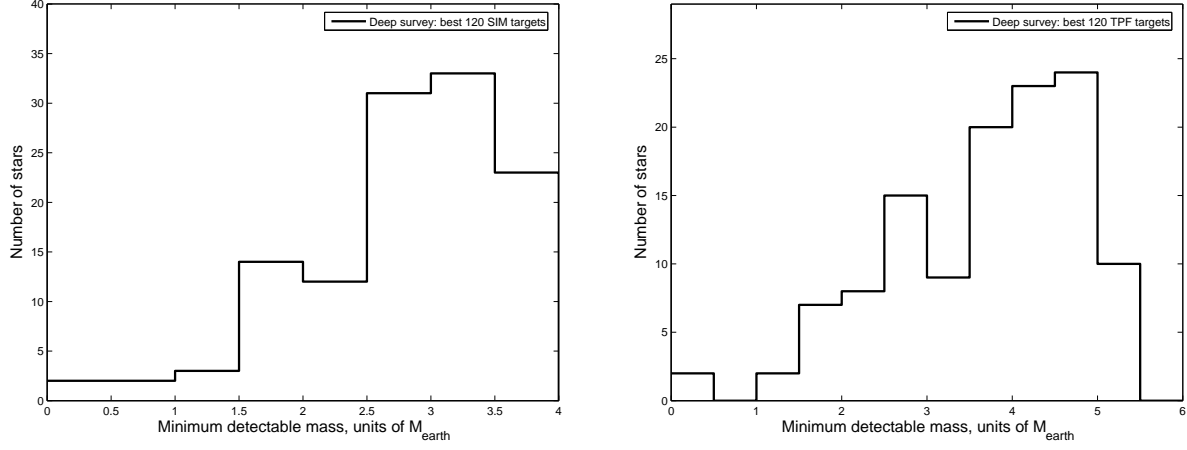


Fig. 11.— Distribution of minimum detectable masses. Left: Deep planet survey – best 120 stars for SIM. Right: Deep planet survey – best 120 stars for TPF. For both plots, there are 104 two-dimensional measurements per star, with single measurement precision  $1.0 \mu\text{as}$ , and minimum detectable mass is for 50% detection efficiency at detection threshold corresponding to 1% false-alarm probability.

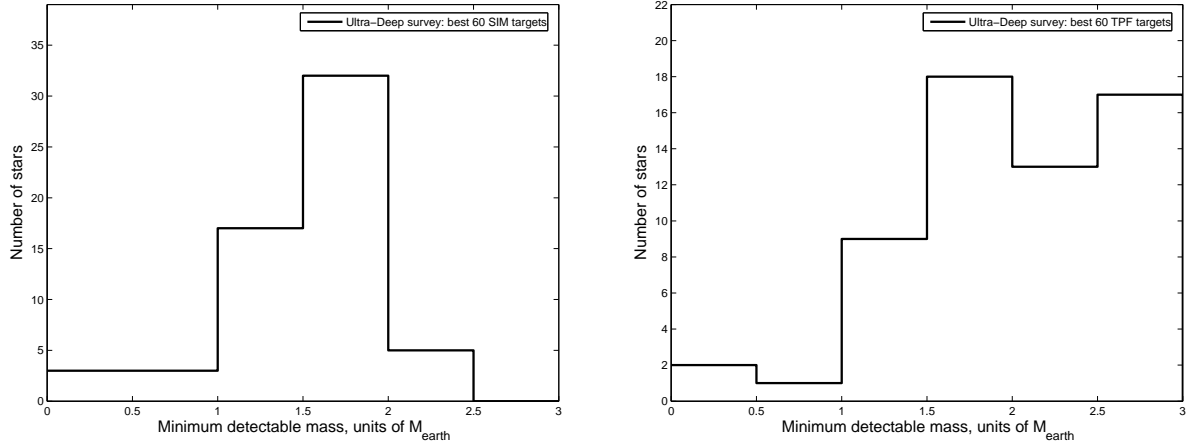


Fig. 12.— Distribution of minimum detectable masses. Left: Ultra-Deep planet survey – best 60 stars for SIM. Right: Ultra-Deep planet survey – best 60 stars for TPF. For both plots, there are 208 two-dimensional measurements per star, with single measurement precision  $1.0 \mu\text{as}$ , and minimum detectable mass is for 50% detection efficiency at detection threshold corresponding to 1% false-alarm probability.

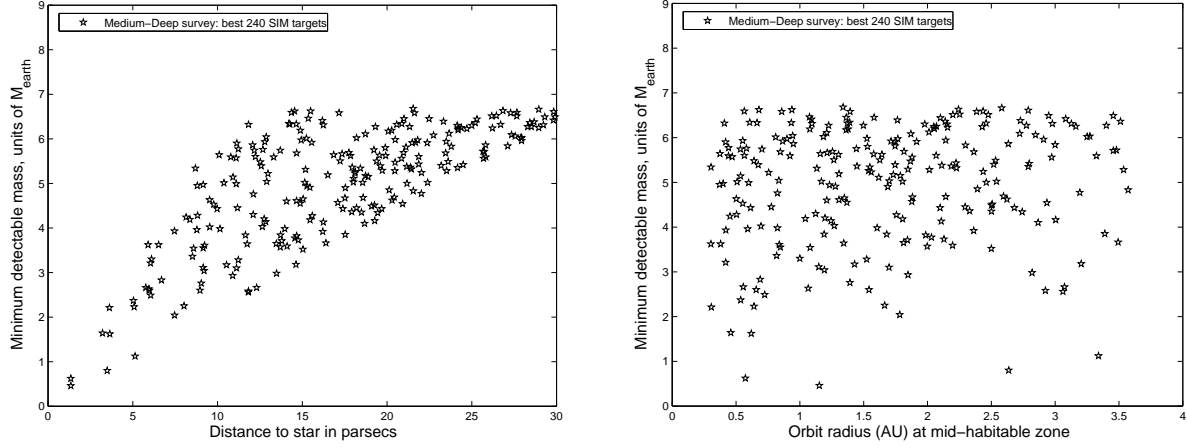


Fig. 13.— Left: Sensitivity versus star distance. Right: Sensitivity versus star-planet separation at mid-habitable zone. Medium-Deep planet survey – 240 stars, 52 two-dimensional measurements per star. For both plots, single measurement precision is  $1.0 \mu\text{as}$ , and minimum detectable mass is for 50% detection efficiency at detection threshold corresponding to 1% false-alarm probability.

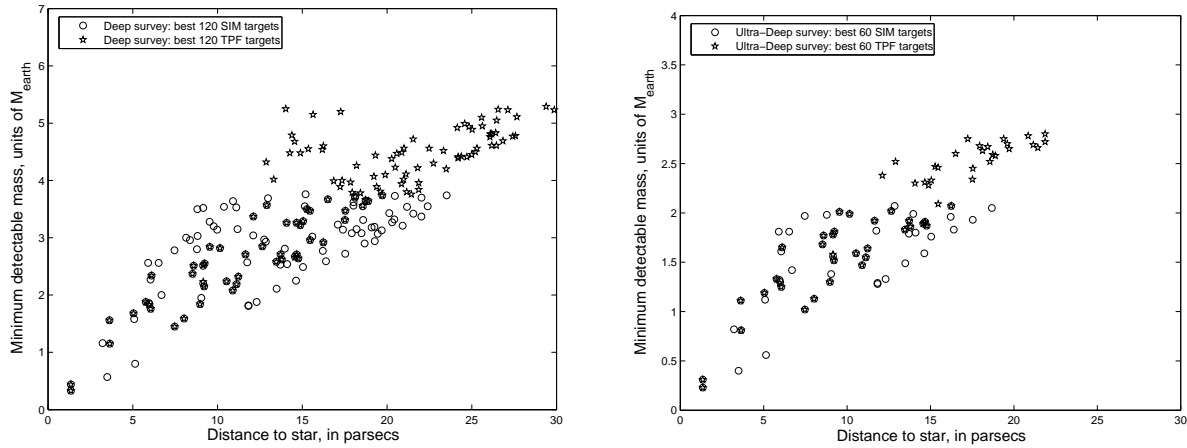


Fig. 14.— Detection sensitivity versus star distance. Left: Deep planet survey – best SIM targets versus best TPF targets: 120 stars, 104 two-dimensional measurements per star. Right: Ultra-Deep planet survey – best SIM targets versus best TPF targets: 60 stars, 208 two-dimensional measurements per star. For both plots, single measurement precision is  $1.0 \mu\text{as}$ , and minimum detectable mass is for 50% detection efficiency at detection threshold corresponding to 1% false-alarm probability.

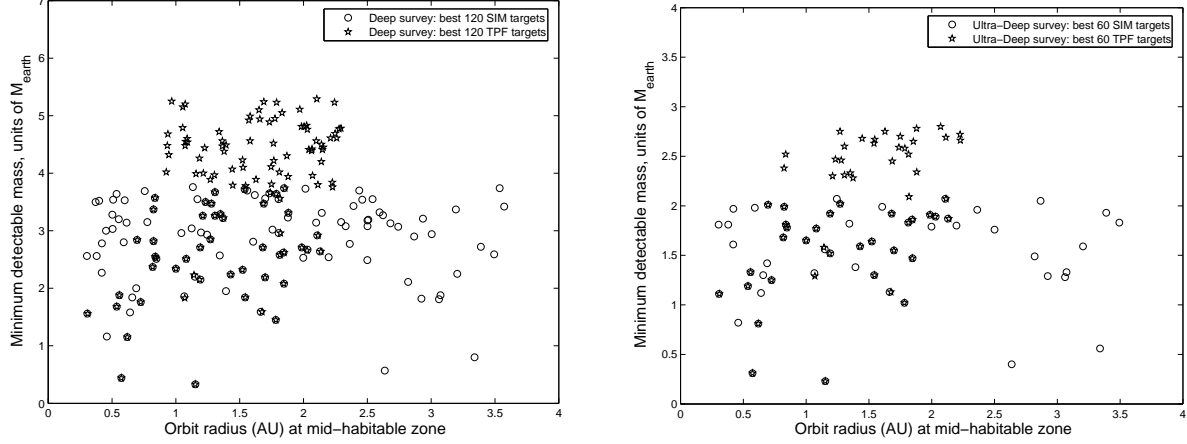


Fig. 15.— Detection sensitivity versus star-planet separation at mid-habitable zone. Left: Deep planet survey – best SIM targets versus best TPF targets: 120 stars, 104 two-dimensional measurements per star. Right: Ultra-Deep planet survey – best SIM targets versus best TPF targets: 60 stars, 208 two-dimensional measurements per star. For both plots, single measurement precision is  $1.0 \mu\text{as}$ , and minimum detectable mass is for 50% detection efficiency at detection threshold corresponding to 1% false-alarm probability.

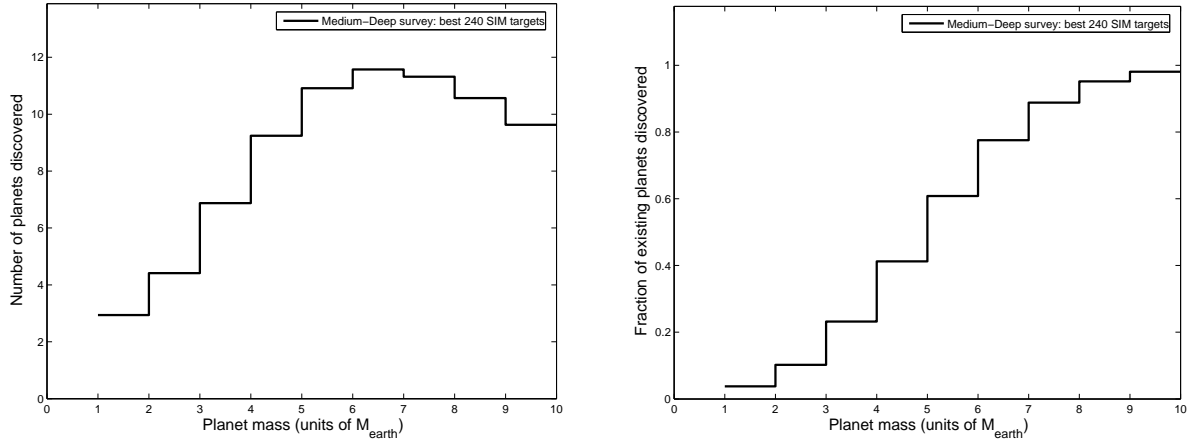


Fig. 16.— Left: Mass distribution of SIM planet discoveries. Right: Completeness – ratio of number of detected planets to number of expected planets, in each mass bin. Both plots are for Medium-Deep planet survey of best 240 SIM targets – 52 two-dimensional measurements per star. Single measurement precision is  $1.0 \mu\text{as}$ ; detection threshold corresponds to 1% false-alarm probability; and planet mass distribution is assumed  $\propto M^{-1.1}$ .

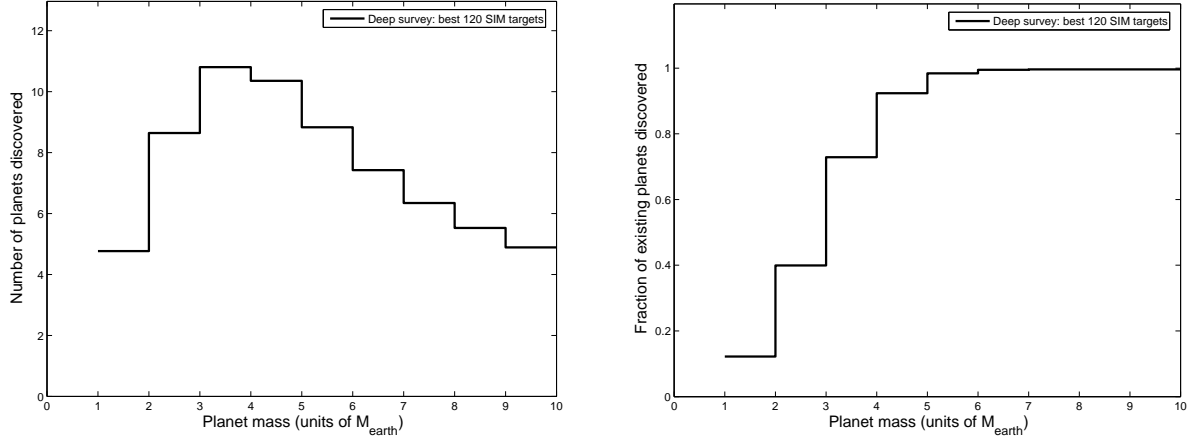


Fig. 17.— Left: Mass distribution of SIM planet discoveries. Right: Completeness – ratio of number of detected planets to number of expected planets, in each mass bin. Both plots are for Deep planet survey of best 120 SIM targets – 104 two-dimensional measurements per star. Single measurement precision is  $1.0 \mu\text{as}$ ; detection threshold corresponds to 1% false-alarm probability; and planet mass distribution is assumed  $\propto M^{-1.1}$ .

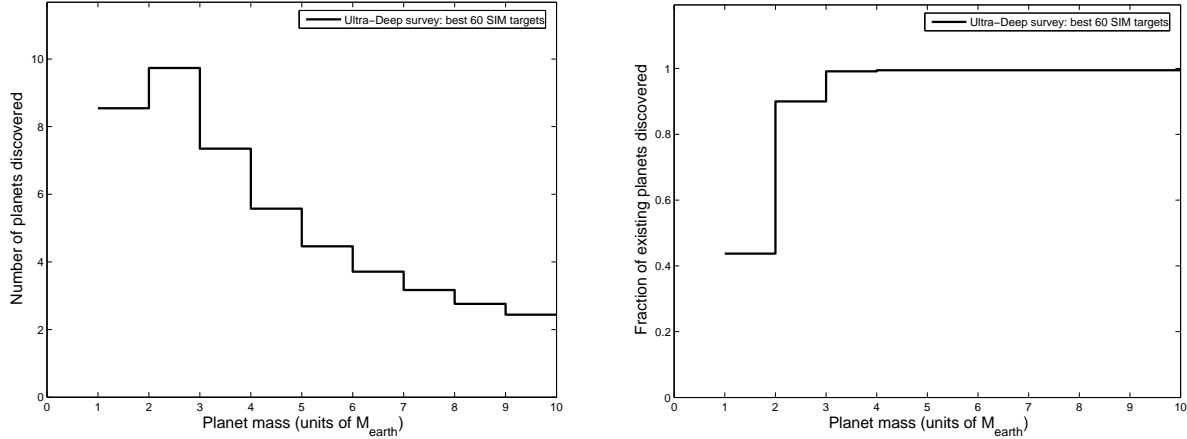


Fig. 18.— Left: Mass distribution of SIM planet discoveries. Right: Completeness – ratio of number of detected planets to number of expected planets, in each mass bin. Both plots are for Ultra-Deep planet survey of best 60 SIM targets – 208 two-dimensional measurements per star. Single measurement precision is  $1.0 \mu\text{as}$ ; detection threshold corresponds to 1% false-alarm probability; and planet mass distribution is assumed  $\propto M^{-1.1}$ .

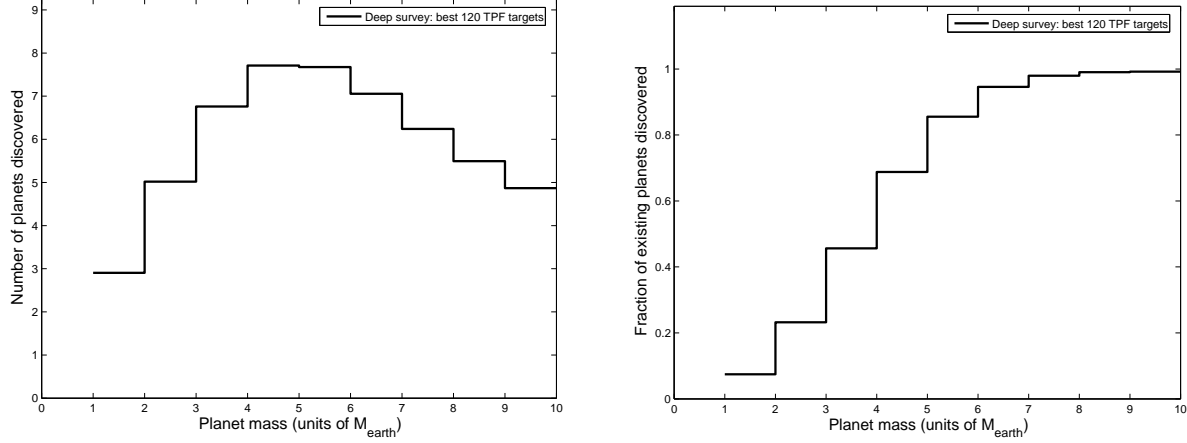


Fig. 19.— Left: Mass distribution of SIM planet discoveries. Right: Completeness – ratio of number of detected planets to number of expected planets, in each mass bin. Both plots are for Deep planet survey of best 120 TPF targets – 104 two-dimensional measurements per star. Single measurement precision is  $1.0 \mu\text{as}$ ; detection threshold corresponds to 1% false-alarm probability; and planet mass distribution is assumed  $\propto M^{-1.1}$ .

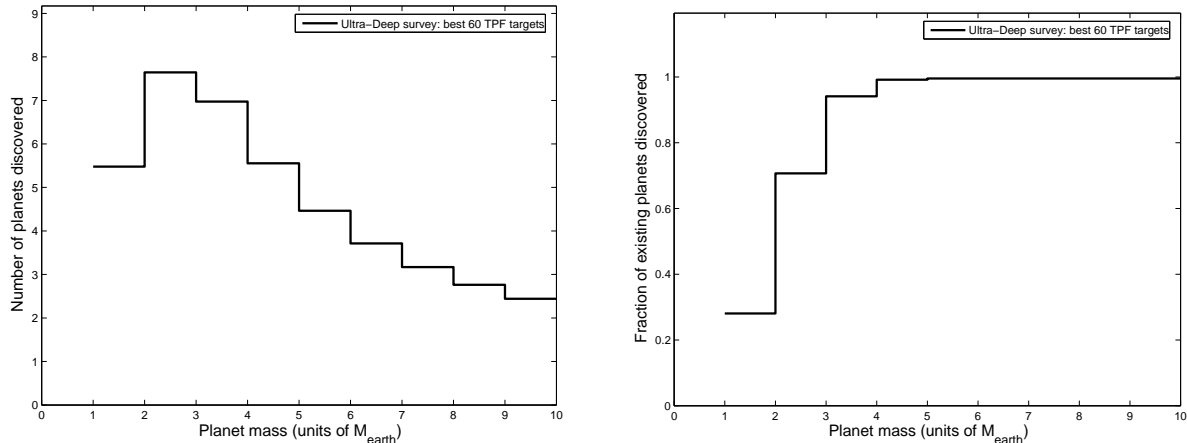


Fig. 20.— Left: Mass distribution of SIM planet discoveries. Right: Completeness – ratio of number of detected planets to number of expected planets, in each mass bin. Both plots are for Ultra-Deep planet survey of best 60 TPF targets – 208 two-dimensional measurements per star. Single measurement precision is  $1.0 \mu\text{as}$ ; detection threshold corresponds to 1% false-alarm probability; and planet mass distribution is assumed  $\propto M^{-1.1}$ .

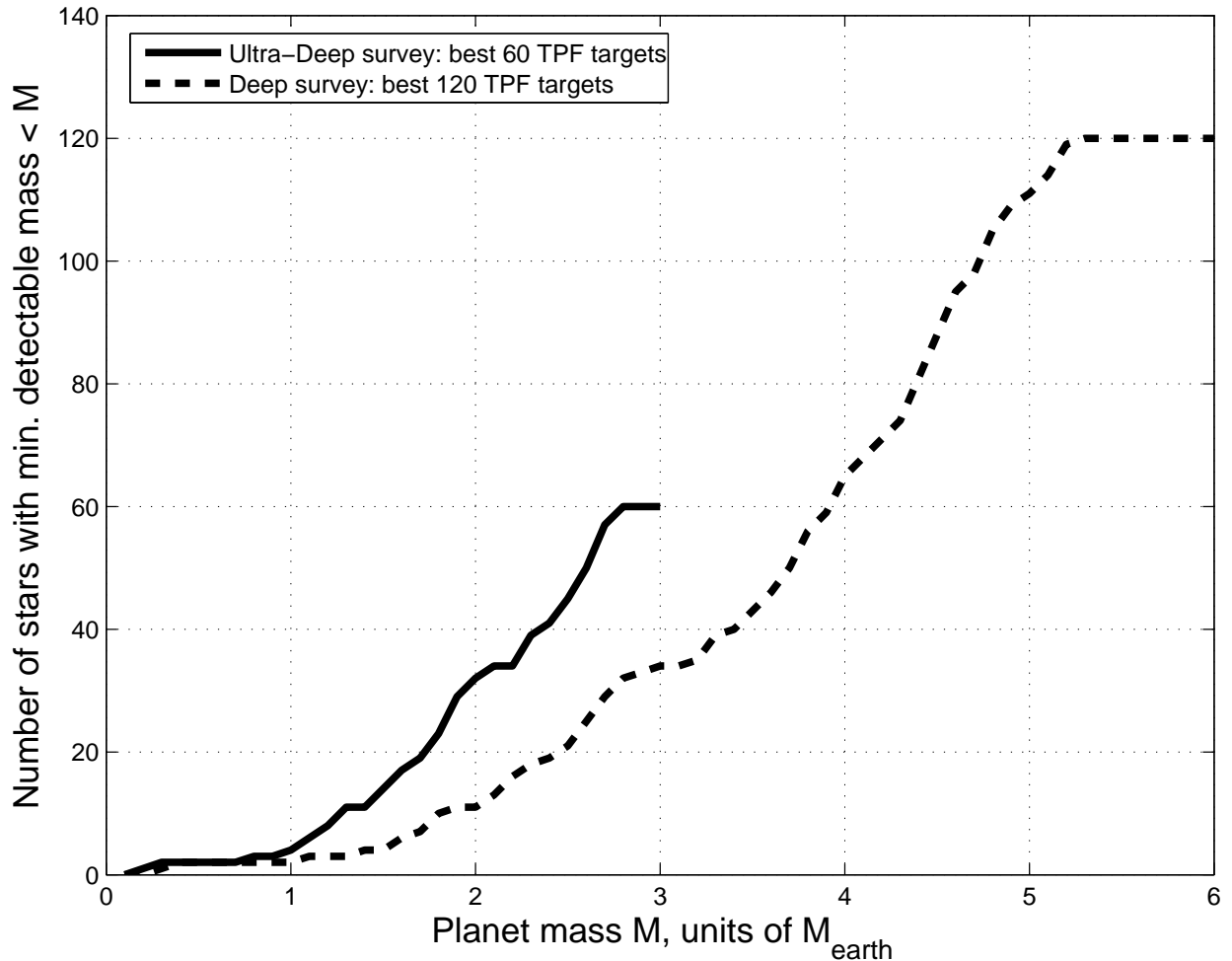


Fig. 21.— SIM planet mass detection limits. Cumulative distribution of minimum detectable mass, for surveys of the best TPF targets. Single measurement precision is  $1.0 \mu\text{as}$ , and minimum detectable mass is for 50% detection efficiency at detection threshold corresponding to 1% false-alarm probability. These results are *independent* of assumptions regarding the mass distribution and occurrence rate of terrestrial planets.

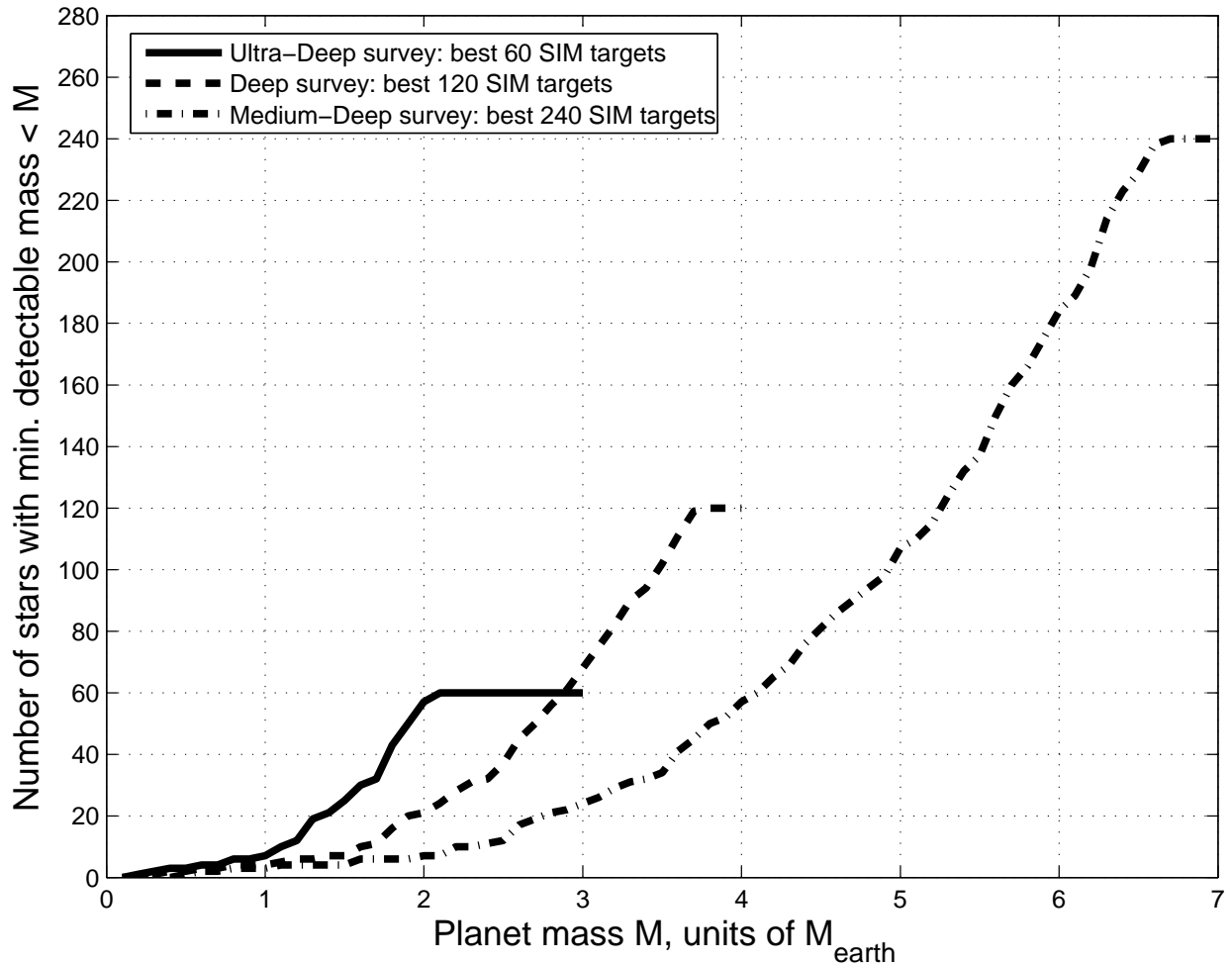


Fig. 22.— SIM planet mass detection limits. Cumulative distribution of minimum detectable mass, for surveys of the best SIM targets. Single measurement precision is  $1.0 \mu\text{as}$ , and minimum detectable mass is for 50% detection efficiency at detection threshold corresponding to 1% false-alarm probability. These results are *independent* of assumptions regarding the mass distribution and occurrence rate of terrestrial planets.

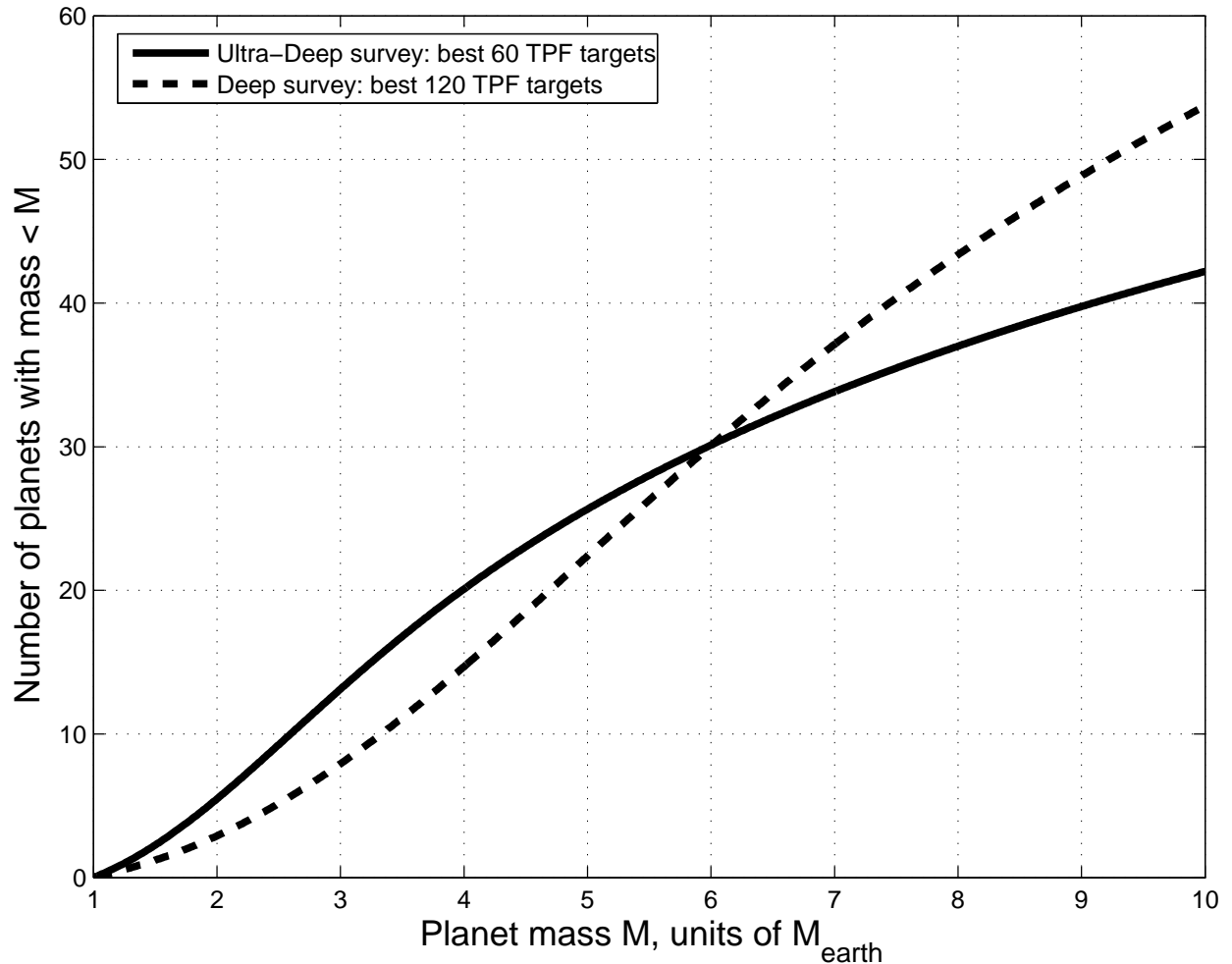


Fig. 23.— SIM planet discoveries. Cumulative distribution of detected planet masses, for surveys of the best TPF targets. Single measurement precision is  $1.0 \mu\text{as}$ , and detection threshold corresponds to 1% false-alarm probability. Assumes that every target star has one terrestrial planet and that the planet masses are distributed as  $M^{-1.1}$ .

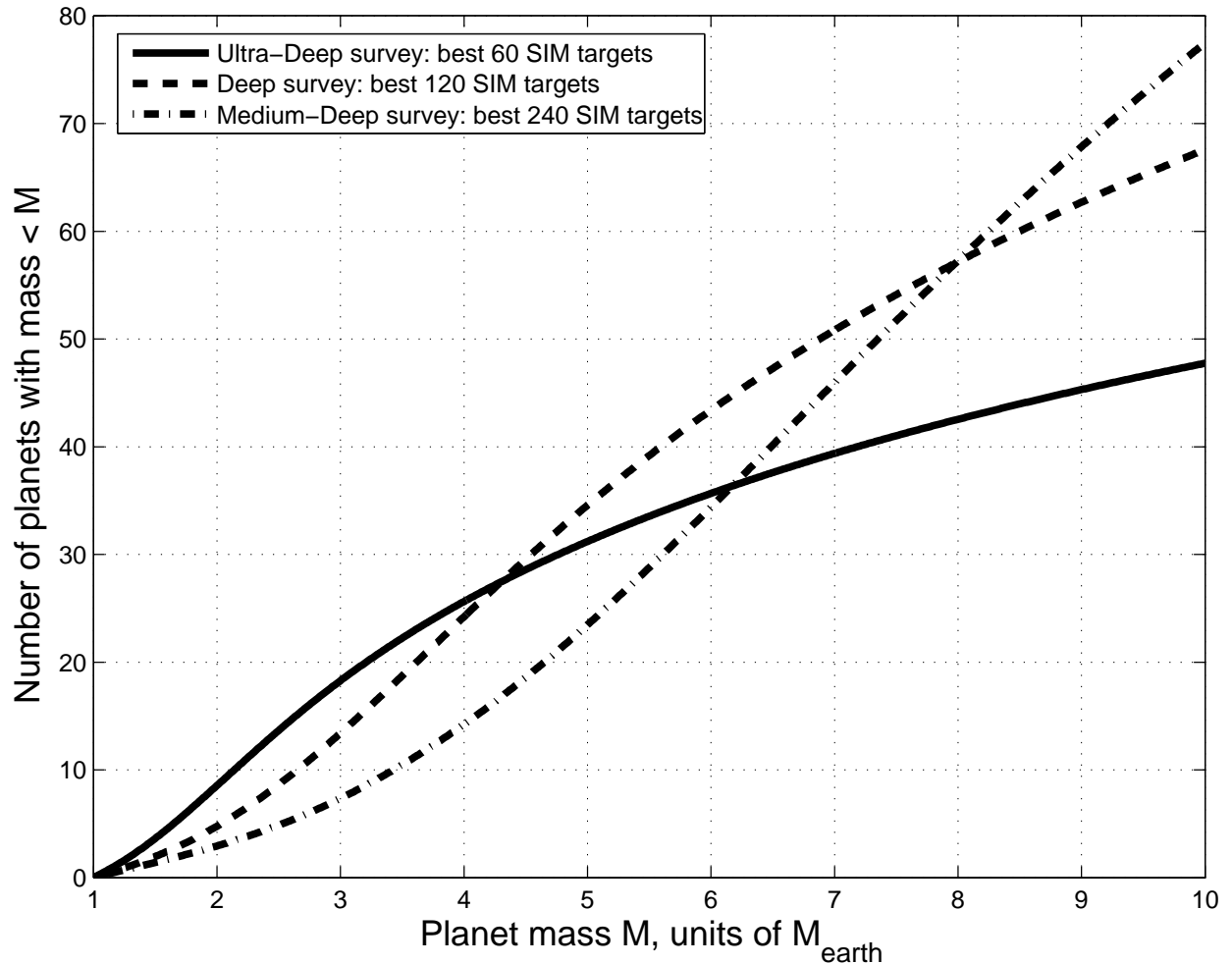


Fig. 24.— SIM planet discoveries. Cumulative distribution of detected planet masses, for surveys of the best SIM targets. Single measurement precision is  $1.0 \mu\text{as}$ , and detection threshold corresponds to 1% false-alarm probability. Assumes that every target star has one terrestrial planet and that the planet masses are distributed as  $M^{-1.1}$ .

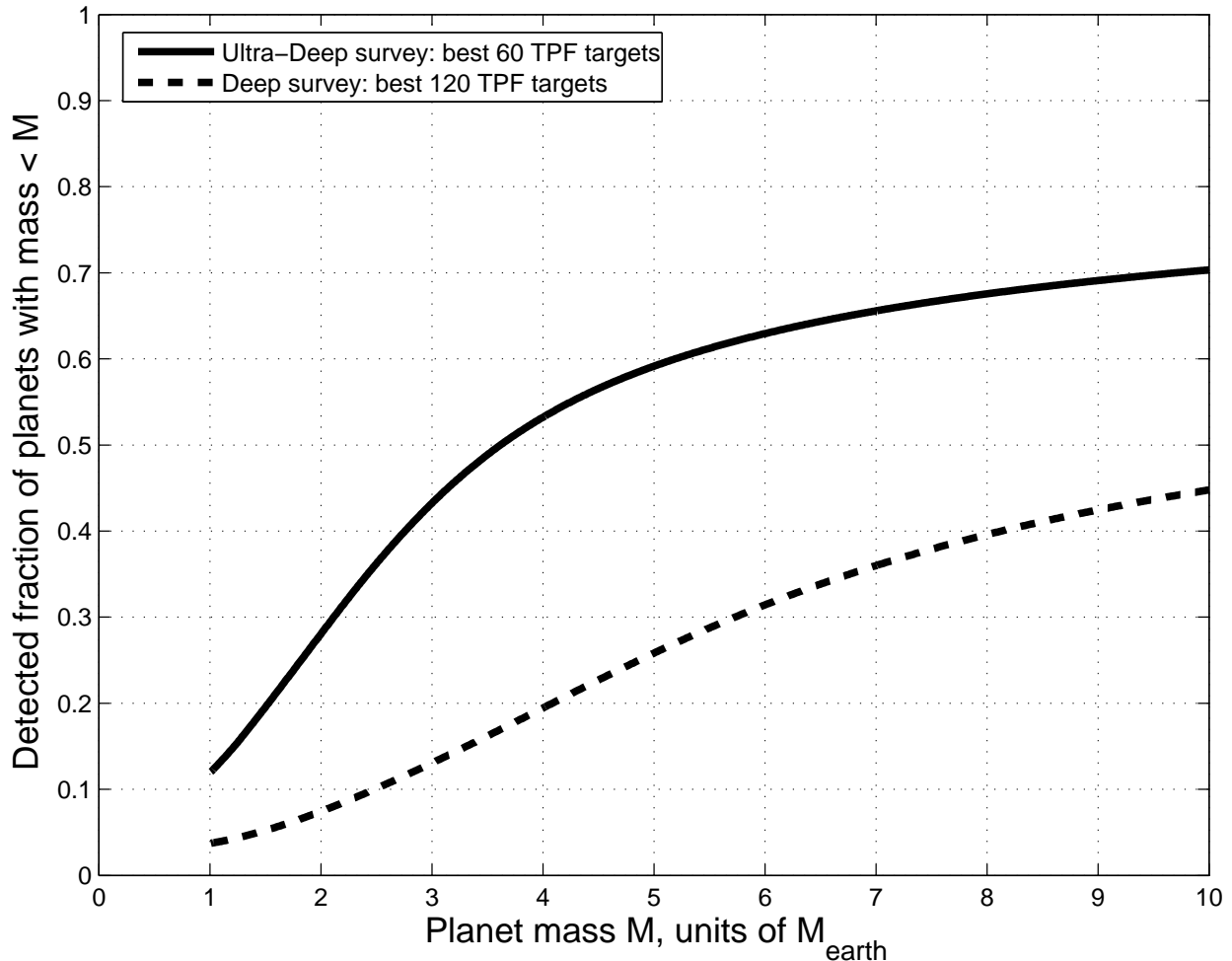


Fig. 25.— Cumulative completeness of SIM planet discoveries, for surveys of the best TPF targets. Cumulative completeness is the ratio of number of detected planets with mass  $< M$  to number of expected planets with mass  $< M$ . Single measurement precision is  $1.0 \mu\text{as}$ , and detection threshold corresponds to 1% false-alarm probability. Assumes that every target star has one terrestrial planet and that the planet masses are distributed as  $M^{-1.1}$ .

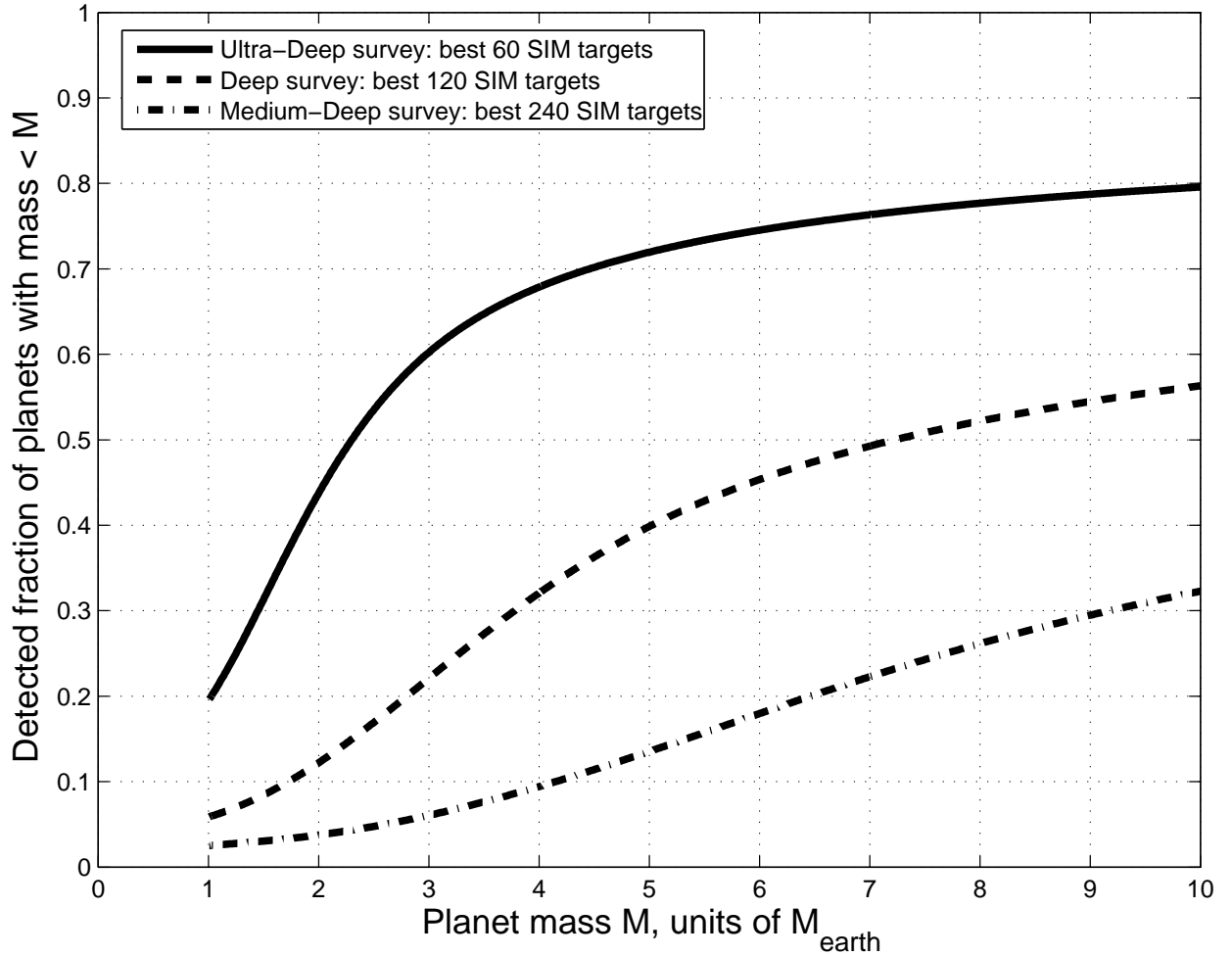


Fig. 26.— Cumulative completeness of SIM planet discoveries, for surveys of the best SIM targets. Cumulative completeness is the ratio of number of detected planets with mass  $< M$  to number of expected planets with mass  $< M$ . Single measurement precision is  $1.0 \mu\text{as}$ , and detection threshold corresponds to 1% false-alarm probability. Assumes that every target star has one terrestrial planet and that the planet masses are distributed as  $M^{-1.1}$ .

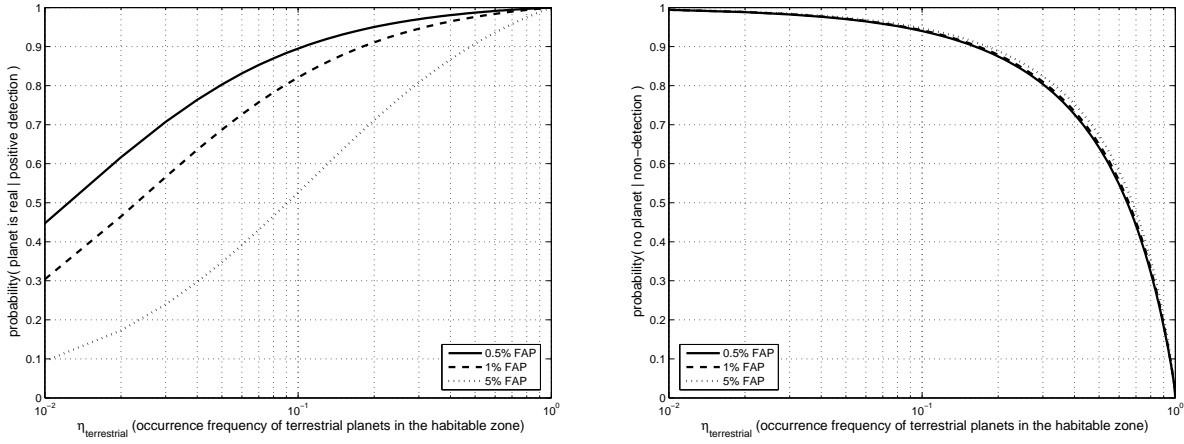


Fig. 27.— Left: Confidence in the *presence* of a terrestrial planet, given a detection. Right: Confidence in the *absence* of a terrestrial planet, given a non-detection. Both plots are for Deep planet survey of best 120 TPF targets – 104 two-dimensional measurements per star, at single measurement precision of  $1.0 \mu\text{as}$ , and show results for detection thresholds corresponding to false-alarm probabilities of 0.5%, 1%, and 5%. Planet mass distribution is assumed  $\propto M^{-1.1}$ . Abscissa is the occurrence rate of terrestrial planets in the habitable zone. Results shown are averaged over all the stars in the survey.